High Temperature Thermal Energy Storage

ME55035 ME-EFPT MSc Thesis

Akash Vishwas Patil

Delft University of Technology

High Temperature Thermal Energy Storage

by

Akash Vishwas Patil

to obtain the degree of Master of Science
at the Delft University of Technology,
to be defended publicly on Tuesday August 27, 2024 at 3:00 PM.

Student number:	5776139	
Project duration:	November 17, 2023 – August 27, 2024	
Thesis committee:	Prof. dr. ir. K. Hooman,	TU Delft, supervisor
	Dr. E. Zanetti,	TU Delft, co-supervisor
	Dr. J.W.R. Peeters ,	TU Delft

TU Delft

Abstract

This study delves into the critical necessity of long-duration energy storage to ensure the consistent reliability of electricity derived from renewable sources. Numerous technologies have emerged to address this need, enabling the storage of surplus energy generated by renewables in diverse materials, taking the forms of sensible or latent heat. The comprehensive analysis explores these various techniques in detail, providing a thorough examination of their respective advantages and disadvantages.

High-temperature TES emerges as a pivotal component, particularly within CSP. This storage capability becomes imperative for maintaining a seamless and predictable power generation process, especially during periods of limited or intermittent sunshine, coinciding with high electricity demand and costs. Presently, CSP plants predominantly employ sensible energy storage in molten salt, a method requiring substantial salt volume, two large tanks or a single tank system. A detailed study is conducted on a similar type of TES system using a PCM as an insulation to minimize the heat losses from the storage tank. The impact of the PCM layer in minimizing the heat loss is analyzed via an analytical model and CFD simulations. The cost incurred for the PCM is further compared with the cost of electrical heating.

Contents

List of Figures

Nomenclature

Abbreviations

Abbreviation	Definition
TES	Thermal energy storage
CSP	Concentrating solar power plants
IEA	International Energy Agency
LCOE	Levelized cost of electricity
HTF	Heat transfer fluid
SHS	Sensible Heat Storage
PCM	Phase change material
HX	Heat Exchanger

Symbols

Symbol	Definition
ΔH_a	Energy of adsorption/absorption
ΔH_v	Energy required for phase change evaporation of the working fluid
ΔH_b	Bonding energy of the working fluid to the sorbent
ρ	Density
c	Specific heat
k	Thermal conductivity
μ	Dynamic viscosity
ν	Kinematic viscosity
α	Thermal diffusivity
β	Thermal Expansion Coefficient
T	Temperature
E	Energy density of the salt
H	Height of the tank
D	Diameter of the tank
th	Thickness of the tank
$\mathrm{m_{ms}}$	mass of molten salt
$\mathrm{cp_{ms}}$	specific heat of molten salt
$\mathrm{cp_{pcm}}$	specific heat of pcm
$\mathrm{T_{ms1}}$	temperature of molten salt at current time step

Symbol	Definition
T_{ms0}	temperature of molten salt at previous time step
R_{ms}	resistance of molten salt
T_{w1}	temperature of wall 1 at current time step
R_{air}	resistance of air
T_{pcm1}	temperature of pcm at current time step
T_{pcm0}	temperature of pcm at previous time step
m_{pcm}	total mass of pcm layer
R_{pcm}	resistance of pcm layer
m_{sol_pcm1}	mass of solid layer of pcm at current time step
m_{sol_pcm0}	mass of solid layer of pcm at previous time step
h_f	latent heat of melting of pcm
T_{w2}	temperature of wall 2 at current time step
m_{liq_pcm1}	mass of liquid layer of pcm at current time step

1

Introduction

In the last decade, there has been a noteworthy shift in the global energy landscape, with renewable sources gaining prominence and contributing significantly to the electricity supply. Between 2011 and 2021, the share of renewable energy in the global electricity mix increased from 20% to 28%, while fossil energy use decreased from 68% to 62%.[16][4] This shift is accompanied by a decline in nuclear energy's contribution from 12% to 10%. Within the renewable energy sector, hydropower witnessed a slight decrease from 16% to 15%, while solar and wind power surged from 2% to 10%. Biomass and geothermal energy also saw growth from 2% to 3%.[16][4]

The burgeoning demand for clean energy, driven by environmental concerns and the imperative to mitigate global warming, has propelled extensive research and development efforts in the field of renewable energy sources. The United States Department of Energy, recognizing the importance of clean energy, actively supports research initiatives, particularly in solar energy. The installed capacity of solar energy has shown a remarkable increase from 41,545 MW in 2010 to 584,842 MW in 2019, accompanied by a substantial rise in actual energy production.[18]

Globally, over 10 million jobs are associated with the renewable energy industries, with China accounting for a significant portion of the recent surge in renewable electricity. With the continuous advancement in efficiency and cost-effectiveness, renewable energy systems are becoming more prevalent, comprising a substantial share of newly installed electricity capacity worldwide.[7] In numerous countries, photovoltaic solar and onshore wind are emerging as the most economically viable options for new electricity installations.

As nations strive towards sustainable energy practices, some have already achieved remarkable milestones, with renewable energy contributing more than 20% to their total energy supply. The projections for the renewable energy market in the coming years indicate continued growth, aligning with global efforts to achieve net-zero emissions by 2050. According to the IEA, 90% of global electricity generation needs to come from renewable sources to meet this ambitious target. Some studies even suggest the feasibility and economic viability of a complete global transition to 100% renewable energy across all sectors.[4]

Renewable energy sources, while abundant and globally stable, grapple with challenges related to low energy density and intermittent availability. For instance, solar energy, despite its widespread availability, faces limitations during nighttime, cloudy weather, and the winter season. Consequently, the integration of an effective energy storage system becomes imperative to mitigate the variability in renewable energy production, ensuring continuous power generation during periods of shortage or increased demand.

Energy storage encompasses various methods, including thermal and chemical approaches. TES stands out as a promising solution, involving the alteration of material internal energy through temperature changes, as seen in sensible heat storage, or phase transitions, as observed in latent heat storage. Chemical storage, on the other hand, utilizes reversible endothermic chemical reactions for energy storage.

The demand for TES systems has surged in response to the escalating energy production from intermittent sources like solar and wind. Notable TES options include latent heat storage, thermo-chemical heat storage, and sensible heat storage in both solid and liquid mediums. As the world grapples with concerns over climate change, pollution, and non-renewable resource depletion, sustainable energy research remains pivotal. CSP plants are emerging as a viable sustainable energy alternative, utilizing solar energy to generate electricity through technologies like solar power towers, parabolic trough collectors, and linear Fresnel reflectors. While these systems excel in areas with high solar irradiation, the variability of solar energy availability and the associated high LCOE present challenges. Herein lies the significance of TES in mitigating such variability and reducing costs. However, efficient storage and recovery of thermal energy are paramount to achieving high capacity factors and a low LCOE.[4]

Molten salt heat storage offers a very sustainable and effecient heat storage option over thermal oil as it can store more heat due to its high heat capacity,has a higher working temeperautre and causes no pollution or fire hazards. On the contrary, there are higher thermal losses in this type of system and also it requires a more complex solar field design.[1]

This study aims to delve into the realm of high-temperature thermal energy storage, exploring its critical role in addressing the challenges posed by variable renewable energy sources. The main research question for this study is to analyze the minimization in the heat loss through a molten salt heat storage tank by using a PCM as an insualtion. We compare the difference in the retention time of the molten salt with and without the PCM insulation via an analytical model and then further validate these results with CFD simulations in Ansys Fluent. As we navigate through various TES technologies, considering factors like energy density, heat transfer efficiency, stability, cost-effectiveness, and reversibility, the study aims to contribute valuable insights to the evolving landscape of sustainable energy solutions. The goal is to minimize the dependency on external heating by offering a sustainable and cost effective alternative.

2

Curent TES Technologies

Within the context of high-temperature thermal energy storage, a comprehensive system comprises three essential components: the storage medium, the heat transfer mechanism, and the containment system. The storage medium serves as the repository for thermal energy, manifesting in various forms such as sensible heat, latent heat of fusion or vaporization, and reversible chemical reactions. Depending on the type of storage, several requirements must be considered to ensure optimal storage dynamics and longevity. These requirements have been identified as:

- High energy density in the storage material
- Good heat transfer between the HTF and the storage medium
- Mechanical and chemical stability of the storage material
- Chemical compatibility between HTF, heat exchanger, and the storage medium
- Complete reversibility for a large number of charging/discharging cycles
- Low thermal losses and cost
- Low environmental impact.

Here is an overview of these thermal energy storage technologies:

2.1. Sensible Heat Storage

Sensible heat storage materials exhibit no phase change throughout the temperature range encountered during the storage process. They efficiently store thermal energy through the sensible heat of solid or liquid materials. This method stands out as the most traditional, well-established, and widely adopted solution for TES owing to its straightforward operation and reasonable cost. However, it is characterized by lower energy storage density compared to alternative TES options.

In this approach, the storage medium—whether liquid (water, oil, etc.) or solid (sand, rock beds, brick) experiences a change in temperature corresponding to the energy transfer (as heat) during both sensible heating and cooling processes.[15] Fig2.1 depicting SHS illustrates the typical profile during these cycles, emphasizing the absence

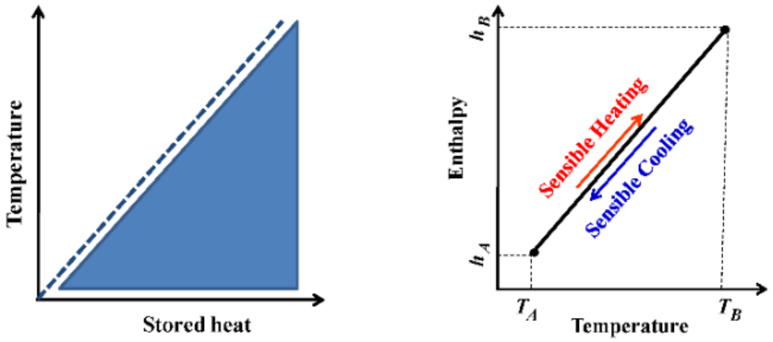

Figure 2.1: SHS diagram with no phase change

of any phase transition throughout the operation.

An advantageous aspect of sensible heat storage is its capacity for repeated cycles of charging and discharging without complications, making it suitable for applications requiring large volumes to meet energy demands. Furthermore, this method optimally utilizes specific properties of the storage material, such as its high specific heat, enhancing overall system efficiency. This literature study explores and analyzes the intricacies of high-temperature sensible heat storage, considering its historical significance, operational characteristics, and potential advancements in the context of thermal energy storage technologies.

2.1.1. Two tank TES system:

Two-tank systems in high-temperature thermal energy storage utilize distinct tanks for molten salt storage—one for high temperature and another for low temperature. In this setup, electricity generated from renewables is converted into heat through electrical heaters. The process involves circulating salt from the cold tank through the heaters, elevating its temperature as needed, and storing it in the hot tank for several days. When energy is required, the hot salt is circulated to a heat exchanger, transferring heat to water and producing high-temperature steam. This steam can be directly applied in industrial processes or used to generate electricity and heat through a turbine. The cooled salt is then returned to the cold tank for the subsequent charging cycle. Notably, the design ensures that the hot and cold fluids remain separate, minimizing heat exchange between them. However, drawbacks include the need for two tanks of equal volume and the frequent pressure cycles impacting the sidewalls of both tanks.

Several companies, including HYME, a Danish startup, employ this technique with variations in heat transfer fluids or salts used as storage mediums. HYME distinguishes itself through its innovative use of sodium hydroxide as a storage medium for molten salt. This choice improves thermal properties, reducing the cost and footprint of molten salt storage and presenting a competitive and scalable approach for decarbonizing heat and power generation. Sodium hydroxide, sourced sustainably from saltwater, exhibits higher thermal efficiency and is both non-toxic and non-flammable. These characteristics, coupled with its abundance in nature, make it a promising solution in the landscape of high-temperature thermal energy storage.

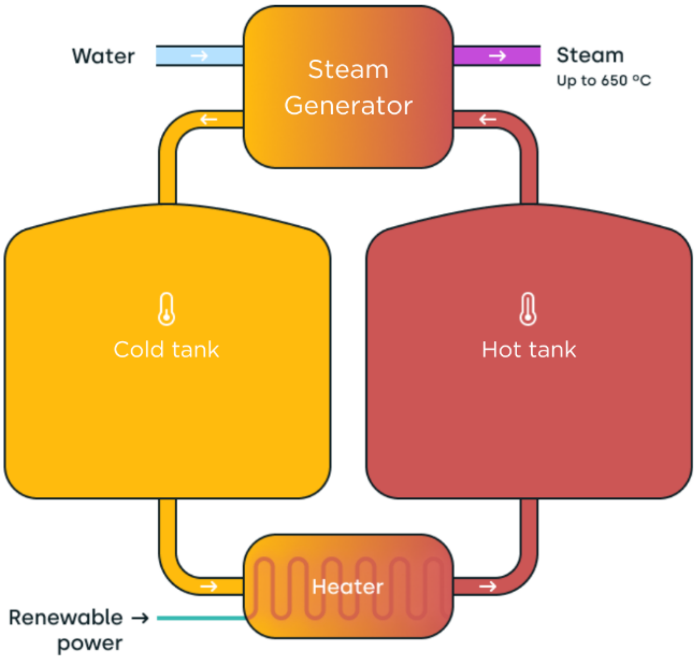

Figure 2.2: Two tank system

2.1.2. Packed bed TES system:

Utilizing solid materials such as rocks or concrete for the storage and release of heat is a common strategy in high-temperature TES systems. The thermal energy storage medium can be either fluid, such as water or molten salt, or solid, encompassing materials like rocks, alumina, silica, concrete, and sand.[10] Single-tank sensible heat storage, while cost-effective and straightforward, faces challenges related to the dropping outlet temperature during the discharging process.Charging the bed involves the flow of fluid, heated by solar radiation, through the packed bed to heat the storage material. The discharge process, aimed at recovering stored energy, entails reversing the flow direction, allowing low-temperature fluid to enter the preheated bed. The exiting fluid, now at a higher temperature, can be effectively utilized in power cycles.

The formation of a thermocline, either by storing the HTF in a single tank or passing it through solid storage media like those mentioned above, is a prominent technique.[14][15] Solid storage configurations often adopt a packed bed arrangement, and the thermocline is influenced by various parameters such as mass flow rate, HTF characteristics, thermal wall losses, and particle size. Achieving a perfect thermocline during the charging process is crucial for maximizing exergy efficiency in single-tank storage.

In the realm of packed-bed TES systems, literature has extensively covered parameters affecting the thermocline, including heat transfer fluid, inlet temperature, packed bed type (design, shape, and orientation), pressure, flow rate, heat storage type (sen-

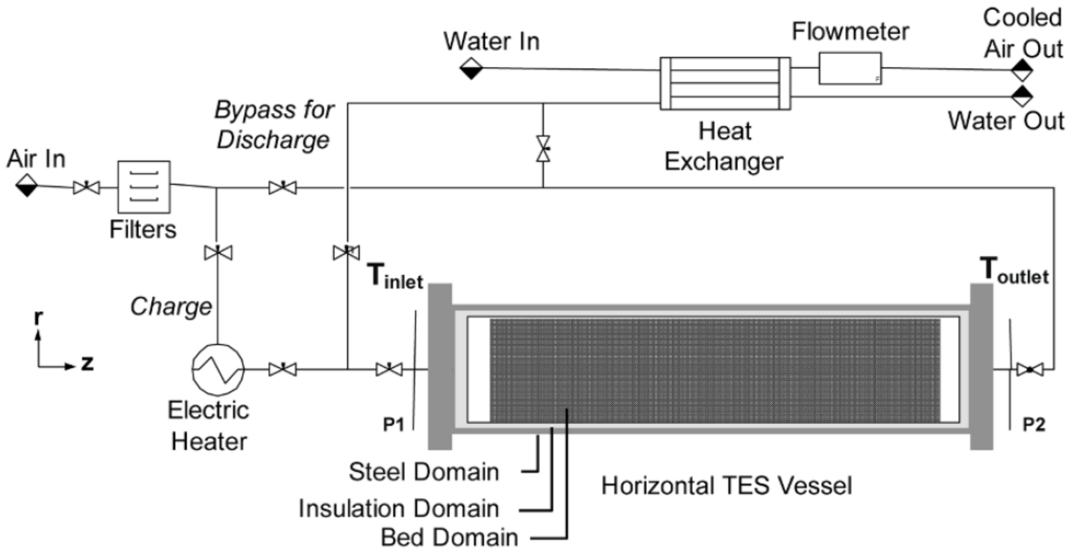

[7]

Figure 2.3: Packed bed system

sible, latent, or a combination), and characteristics of storage materials (type, size, and shape of solid particles). The choice of storage medium type is contingent on factors like application type, thermophysical properties, and cost considerations.

Numerous studies have explored the impact of different storage materials on thermal performance, with considerations for factors like energy stored, exergy to energy ratio, and particle size effects on pressure drop and temperature gradient. The size and shape of solid particles, as well as their void fraction, play crucial roles in thermal stratification, efficiency, and pressure drop losses. Achieving a balance between thermophysical properties, shape, size, type, and cost of storage materials is pivotal.

Materials exhibiting favorable thermal properties, such as high thermal conductivity and volumetric heat capacity, coupled with cost-effectiveness, are deemed optimal for practical applications. In addition to the thermophysical properties, the cost of storage materials must be considered for a cost-effective thermal energy storage system. The cost of a TES system includes the storage vessel, insulation and solid materials. Inexpensive materials can lower the total cost in renewable energy applications such as CSP plants, helping to meet the US DOE Solar Energy Technologies Office's electricity cost goal of $0.05/kWh in 2030.[3]

Alumina Energy, a prominent developer specializing in particle packed bed thermal energy storage technology for extended and utility-scale energy storage, has introduced a cutting-edge approach to store and recover thermal energy at temperatures reaching up to 1,600 $^\circ C$. This innovative method employs cost-effective, high-temperature stable ceramic particles in a packed bed design, offering distinct advantages over existing thermal energy storage systems in terms of performance and implementation.

The utilization of a packed bed with high-temperature stable, low-cost, and entirely recycled particle storage materials presents a valuable enhancement for renewable energy systems, contributing to increased flexibility, reliability, and a reduction in the LCOE.[7]

The specific ceramic material employed, known as Rethink Seramic – Flora and commercialized by Seramic Materials Ltd, holds considerable promise for high-temperature TES applications. With an estimated cost ranging from \$800 to \$1000 per ton, ReThink Seramic – Flora emerges as a viable candidate compared to commercial aluminum oxide, which is priced between \$1900 and \$2300 per ton. The quadrilobed shape of the packed-bed filler material is strategically designed to minimize pressure drop, enabling its application in scenarios with temperatures reaching up to 1200 $^{\circ}C$. Although the study assumes an inlet temperature of 150 $^{\circ}C$, it is noteworthy that the stability of ReThink Seramic – Flora extends up to 1250 $^{\circ}C$, positioning it as a prospective material for high-temperature TES applications.[7][4]

(a) Actual dimensions **(b)** Packed bed filler material

Figure 2.4: ReThink Seramic-Flora quadrilobe
[7]

The filler material used in this research is a quadrilobe measuring 18 mm in diameter, featuring a central hole of 4 mm in diameter, with typical lengths ranging from 5 to 12.5 mm. The surface area to volume ratio of ReThink Seramic – Flora is compared with a 6 mm alumina sphere, indicating distinctive characteristics with surface areas of 590 m^2/m^3 and 1000 m^2/m^3, respectively.[7]

2.2. Latent Heat Storage

Storing thermal energy within PCMs, such as inorganic salt mixtures, exploiting the latent heat of fusion, has demonstrated the potential to enhance energy density for storage by up to 50% and significantly reduce costs by over 40%.[21] However, a substantial challenge hindering the widespread commercial adoption of PCM-based TES in CSP systems pertains to the difficulty in discharging the latent heat stored in the PCM melt at specified heat rates.[16]

This challenge arises due to the phenomenon where, during the heat extraction process, the PCM-melt, characterized by low thermal conductivity, solidifies onto the heat exchanger surface. This solidification process leads to a decrease in heat transfer efficiency, necessitating a larger heat transfer area and consequently resulting in higher costs. Achieving consistently high heat rates demands an increase in either the heat transfer area or the heat transfer coefficient.[29]

Numerous investigations have been conducted to improve the heat transfer coefficient; however, these efforts have proven to be largely unsuccessful. This persistent issue underscores the need for innovative solutions to optimize the discharge process of latent heat in PCM-TES for CSP applications, addressing the challenges associated with heat transfer efficiency and cost-effectiveness.[11]

2.2.1. Sacrificial Polymer Method:

The enhancement of PCM efficiency through encapsulation within small capsules offers increased specific surface area. Simultaneously, direct contact with a heat transfer fluid amplifies the heat transfer coefficient. However, a notable technical challenge in encapsulating salts involves the necessity to create a void inside the shell during production. This void is crucial to accommodate volume expansion during melting and heating processes.[16]

In collaboration with the Department of Energy, Terrafore Inc. is actively engaged in research endeavors aimed at innovatively and economically creating this necessary void. The goal is to encapsulate the salt within a shell material capable of withstanding high-temperature thermal cycles, ensuring durability over the thirty-year lifespan of a solar plant.

The primary objective of the project is to manufacture capsules ranging from 5mm to 15mm, containing an inorganic salt mixture for thermal energy storage. This storage involves a combination of latent heat transitioning from solid to liquid and sensible heat. The chosen shell material must demonstrate compatibility with a molten salt heat transfer fluid, heated to temperatures reaching up to 600$^\circ C$. Moreover, it must exhibit robustness to endure over 10,000 thermal cycles spanning temperatures from 300$^\circ C$ to 600$^\circ C$. The project sets a stringent criterion for breakage, aiming for a rate of less than 0.1% per year.[16]

Fig 2.5 illustrates the schematic representation of the methodology employed for creating a void within the capsule. The process initiates with the application of a sacrificial polymer layer onto a salt prill of a chosen diameter, followed by an additional coating comprising a mixture of binder and inorganic shell material. Utilizing a fluid-bed coater, these layers are meticulously applied to the prill. [16]Subsequently, the produced capsule undergoes gradual heating in a furnace, leading to the decomposition of the polymer and organic binder into gas. These gases then escape through the pores of the shell, resulting in the formation of a void surrounding the salt within the capsule.

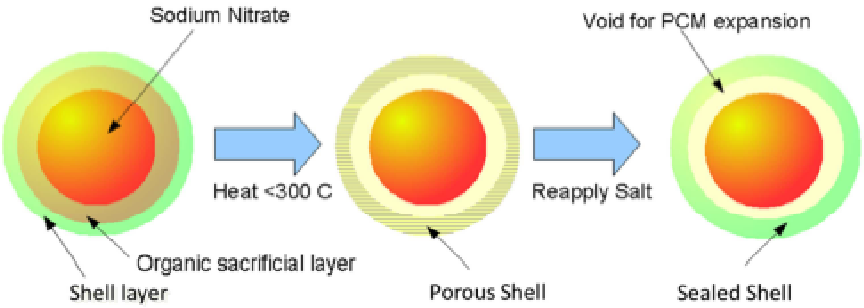

Figure 2.5: A polymer layer between shell and prill is decomposed to gas to create a void in the capsule
[16]

Notably, the fluid bed coating process employed in this procedure is a well-established technique in the industry, requiring no specialized equipment for capsule production. This scientifically devised approach offers a feasible and accessible method for creating voids in capsules, presenting a promising avenue for the advancement of encapsulation techniques in thermal energy storage applications.[16][30]

Figure 2.6 illustrates the schematic representation of a thermal energy storage tank employing a packed bed of PCM capsules immersed in a molten salt HTF, such as a low-melting molten salt mixture. Three distinct PCM salt capsules are depicted in a stacked configuration within the tank, with HTF filling the spaces between the capsules. This cascading arrangement is essential for the efficient utilization of latent heat in PCM.

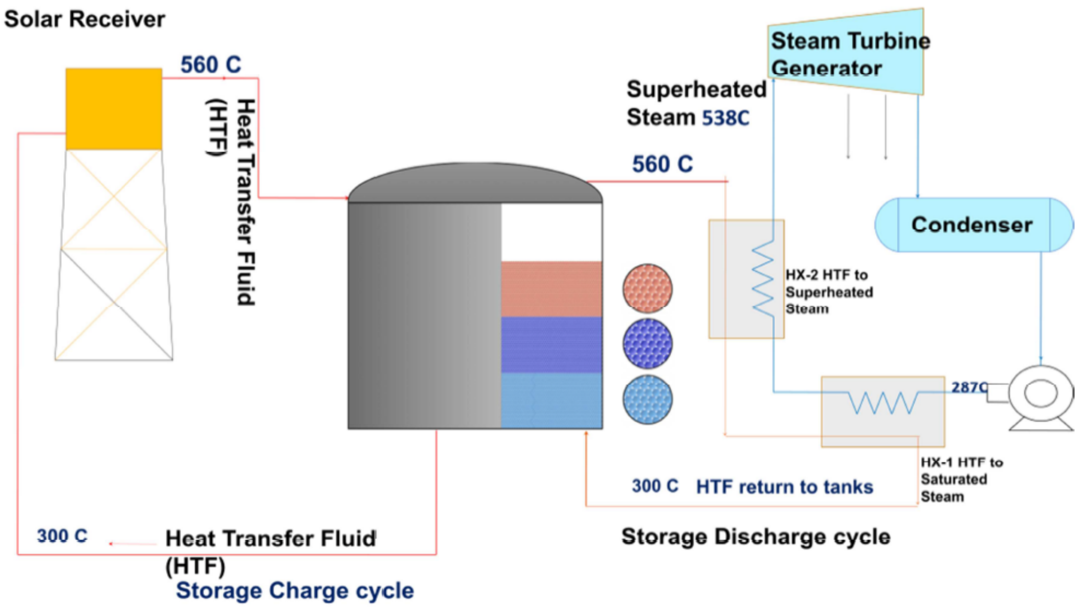

Figure 2.6: Cascaded encapsulated phase change storage tank
[16]

During the storage charge cycle, HTF, collecting heat from a solar collector-receiver (depicted as a tower receiver), is pumped through the packed bed of capsules in the storage tank. The heat is transferred by direct contact with the capsules, initiating the melting of salt and subsequently heating the salt in the capsules to the high operating temperature of HTF. The charged status is achieved when the exit temperature increases by approximately 5% of the difference between the operating temperatures.[16]

In the storage discharge cycle, HTF from the top of the storage tank is pumped through power block heat exchangers, including superheater HX-2 and high-pressure boiler preheater HX-1. This process results in boiling water from the condenser and superheating steam, subsequently used to generate electricity in a steam turbine generator. The cold HTF exiting from the boiler-preheater HX-1 is then returned to the bottom of the storage tank. As HTF flows upward through the tank, it is heated by transferring heat from the salt, which freezes inside the capsules. The discharge is considered complete when the exit temperature decreases by about 5% of the difference between the operating temperatures.

The heat stored inside the capsules includes sensible and latent heat in the PCM salt, in addition to the sensible heat in the HTF occupying the space in the tank not occupied by the capsules. The tank is thermally stratified, with hot HTF fluid at the top and cold fluid at the bottom, maintaining effective thermal stratification due to the high specific heat capacitance of the capsules.

To enhance latent heat utilization and maintain fluid temperature during discharge, a cascading approach is implemented.[20] This involves using progressively higher melting point salts inside the capsules, with the lowest melting point at the bottom and the highest at the top. The selection of the melting points is guided by cut-off point temperatures, representing the end of charge and discharge cycles. The mathematical model used in the analysis suggests significant flexibility in choosing bed materials for middle layers, and the height of the capsule beds can be optimized considering the model and salt costs.

2.3. Thermochemical Energy Storage

Thermal energy storage can be effectively managed using principles of sensible heat, latent heat, and chemical reactions. Chemical reactions between specific materials allow for the storage and release of heat energy in a reversible manner. By supplying heat to certain chemical compounds, their molecular bonds can be broken, allowing them to store heat energy. Conversely, by recombining these components, the stored heat energy can be retrieved for use in heating or cooling applications.

While thermochemical energy storage systems have primarily been developed for space heating in buildings, they hold potential for broader applications. For heating purposes, solar radiation provides ample high-grade heat energy that can be harnessed through solar collectors. Combining thermochemical energy storage with long-term seasonal thermal energy storage systems can further enhance energy efficiency and contribute to environmental sustainability by reducing carbon emissions.

In thermochemical energy storage systems utilizing sorption materials, heat energy is utilized to release water vapor, and subsequently, heat energy is released when the water vapor is absorbed or adsorbed. The sorption material plays a crucial role in shifting the phase equilibrium of the working fluid from vapor-liquid to vapor-condensed phase, thereby facilitating energy storage.

During the charging phase, the supplied heat energy breaks the reversible bonding between the molecules of the working fluid and the sorption material. As a result, the gaseous working fluid is released into the environment in an open system or condensed in a closed system. This process separates the energy and entropy fluxes through the thermochemical storage principle. Upon discharge, the separated reactive components/working fluid pairs are recombined, resulting in the release of entropy. The energy associated with adsorption/absorption can be quantified using the relation:[26]

$$\Delta H_a = \Delta H_v + \Delta H_b \tag{2.1}$$

Four main categories of materials are available for thermochemical energy storage, each of which possesses its own characteristics based on thermophysical properties, and they are:

- Adsorption materials

- Absorption materials
- Pure thermochemical materials
- Composite thermochemical materials

2.3.1. Open adsorption energy storage system:

Open adsorption energy storage presents an appealing option for serving as a heat reservoir to address peak load demands and redistribute energy as needed. Particularly, it holds promise for integration into thermal storage systems within buildings. Researchers at the Institute of Thermodynamics and Thermal Engineering at the University of Stuttgart,[26][28] Germany, have been actively engaged in developing such adsorption energy storage systems. Recently, they have proposed an open adsorption energy storage system, the operational principle of which is depicted schematically in Figure 2.7. Additionally, Figure 2.8 illustrates how this system can fulfill heating demands in building applications.

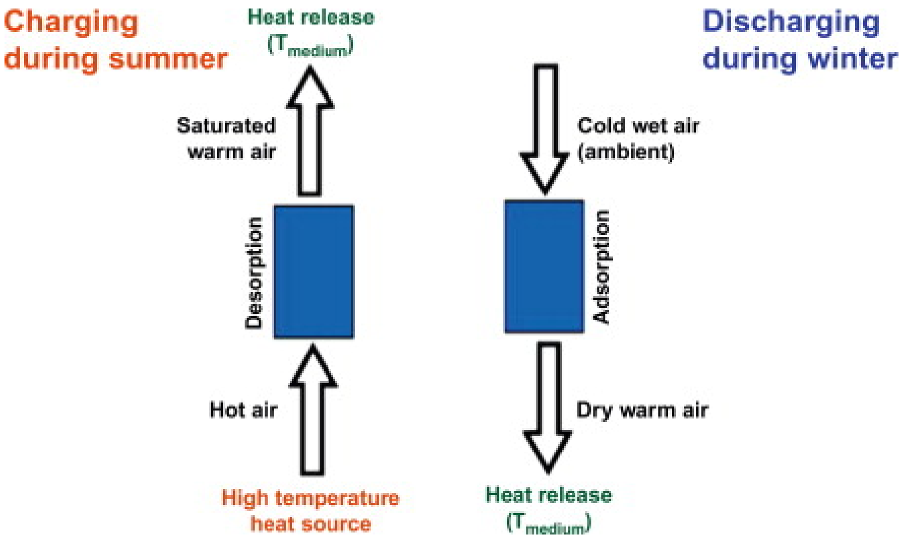

Figure 2.7: Operating principle of an open adsorption energy storage system

During the regeneration cycle, hot air exiting the solar collector, with temperatures ranging between 180 to 190°C, is directed across the energy storage unit. This unit is filled with zeolite 4A material, which undergoes a desorption reaction, capturing the water content present in the material as it interacts with the hot air flow. Simultaneously, the heat from the hot air is transferred to the material, enabling the storage of heat energy within it. Subsequently, the warm air discharged from the thermal store can be utilized for primary heating purposes.

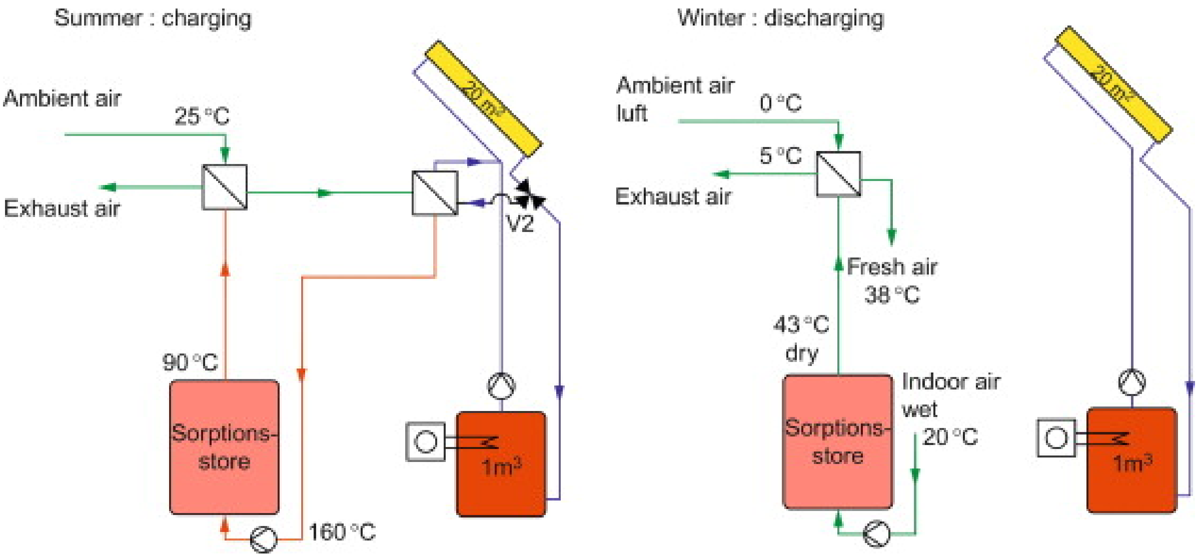

Figure 2.8: Open adsorption thermal storage system for application in buildings

2.3.2. Closed absorption energy storage system:

The operational concept of this system closely resembles that of the closed adsorption system. Solar heat is directly applied to the regenerative heat exchanger containing the low-concentration solution (NaOH solution).[28] This heat input facilitates the separation of water content from the NaOH solution, effectively accomplishing the desorption process. The resulting highly concentrated caustic soda (devoid of water content) is stored separately for future use. Meanwhile, the water vapor generated during desorption is cooled, condensed, and appropriately stored in the sorbate storage tank. Any surplus heat generated is redirected to the ground heat exchanger for storage and subsequent utilization during the winter season.

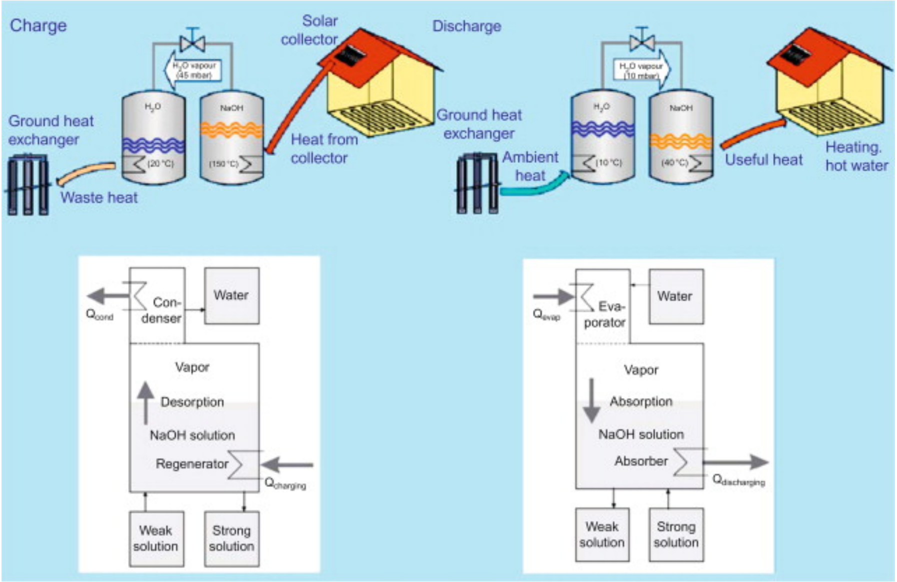

Figure 2.9: Operating principle of closed adsorption energy storage system

During the discharging cycle, the low-temperature heat obtained from the ground heat exchanger is utilized to vaporize the stored water in the sorbate tank. The resulting vapor is then directed to the absorbed tank, where the concentrated caustic soda lye releases the stored heat.

3

Heat Loss Calculations

We consider a TES system that uses molten salt as a storage medium. The salt used is **Solar salt** which consists of 60% $NaNo_3$ and 40% KNO_3. It is widely used in TES systems, particularly in CSP plants, due to its favorable thermal properties and cost-effectiveness. The advantages of using solar salt are[25]:

- Solar salt is thermally stable up to temperatures around 600°C, making it suitable for high-temperature applications. Operating at 565°C ensures a safety margin below its decomposition point, providing reliable and long-term performance without significant degradation.
- The melting point range of the salt is 220°C to 250°C, giving a very wide liquid range of 250°C to 600°C. This allows for a high amount of sensible heat storage.
- Solar salt has a high specific heat capacity, allowing it to store a large amount of thermal energy per unit mass which makes it efficient for sensible heat storage.
- The components of solar salt (sodium nitrate and potassium nitrate) are relatively abundant and cost-effective compared to other high-temperature heat transfer fluids. This makes solar salt an economically viable option for large-scale TES systems.

3.1. Heat loss without PCM

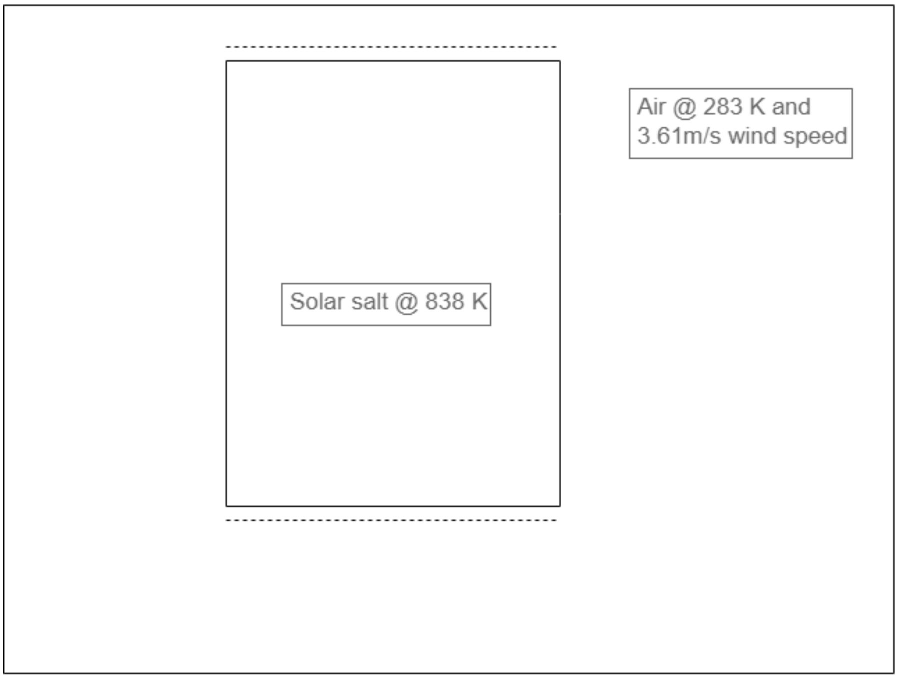

Figure 3.1: Molten salt storage tank

3.1.1. Assumptions:

- The tank is insulated from the top as well as the bottom.
- Only one-dimensional heat transfer is considered.
- The energy requirement is 6000 kWh/day.
- The initial temperature of salt is 838K.[8]
- Outside temperature is 283K and average wind speed is 3.61m/s.[9][5]

3.1.2. Heat Transfer Coefficient:

There are three heat transfer coefficients responsible for natural convection in the molten salt, conduction through the wall of the tank and forced convection with the outside air. The thermophysical properties of the salt are listed in the table below[8]:

Property	Unit	Value
Melting point	$[K]$	519.3
Density	$[kg/m^3]$	1712.33
Specific Heat	$[J/kgK]$	1596.46
Thermal Conductivity	$[W/mK]$	0.5501
Dynamic Viscosity	$[Pas]$	0.0012
Kinematic Viscosity	$[m^2/s]$	7.00799×10^{-7}
Thermal Diffusivity	$[m^2/s]$	2.01232×10^{-7}
Thermal Expansion Coefficient	$[K^{-1}]$	0.00004
Prandtl Number	$[-]$	3.482552263
Grashof No	$[-]$	1.19949×10^{13}

To size the tank to meet the energy requirement, first, the energy density of the salt is calculated by the equation[17]:

$$E = \frac{cT\rho}{3600 * 1000} = \frac{1596.46 * 838 * 1712.33}{3600 * 1000} = 636.3367786kWh/m^3 \tag{3.1}$$

The volume of the tank is calculated by taking the ratio of the total energy requirement to the energy density.

$$V = \frac{\text{Total energy requirement}}{E} = \frac{6000}{636.3367786} = 9.428969379m^3 \tag{3.2}$$

For the first iteration, the diameter of the tank is assumed to be **2m**, and the resultant height is approximately **3m**.

3.1.3. Natural Convection:

To calculate the heat transfer coefficient for natural convection inside the tank, we start the with calculation of the Rayleigh number for the given fluid.[17]

$$Ra = \frac{g\beta \Delta T H^3}{\nu\alpha} = 4.17727 \times 10^{13} \tag{3.3}$$

The vertical cylinder can be treated as a vertical wall when the diameter is sufficiently large so that the curvature effects are negligible.[17] This is true when

$$D \geq \frac{35H}{Gr_H^{1/4}} \tag{3.4}$$

where $Gr_H = \frac{Ra_H}{Pr}$ This condition is satisfied for the given values of diameter and height. Hence, the tank can be modeled as a vertical wall.
The Nusselt number correlation for a vertical wall is given by[17]

$$Nu = \left(0.825 + \frac{0.387 Ra_H^{1/6}}{\left[1 + \left(\frac{0.492}{Pr} \right)^{9/16} \right]^{8/27}} \right)^2 = 3009.413814 \tag{3.5}$$

The value of the heat transfer coefficient is hence given by

$$h_i = \frac{Nu * k}{D} = 551.3012509W/m^2K \tag{3.6}$$

3.1.4. Conduction:

Conductive heat transfer happens through the walls of the storage tank. The material of the tank is a nickel alloy known as Hastelloy which has high corrosion resistance and is stable at high temperatures. The conductive resistance for the tank is given by

$$R = \frac{th}{k} = 0.000909091m^2K/W \tag{3.7}$$

3.1.5. Forced Convection:

Forced convection takes place with air as a wind speed of 3.61m/s is considered[5].The air temperature is considered to be 283K [9]. The thermophysical properties of air at 283K are given in 3.1.5[19]

Property	Unit	Value
Density	$[kg/m^3]$	1.246
Specific Heat	$[J/kgK]$	1005
Thermal Conductivity	$[W/mK]$	0.02512
Dynamic Viscosity	$[Pas]$	0.00001778
Kinematic Viscosity	$[m^2/s]$	1.42697$\times 10^{-5}$
Thermal Diffusivity	$[m^2/s]$	2.00602$\times 10^{-5}$
Prandtl Number	$[-]$	0.711341561
Reynolds No	$[-]$	505968.5039

The Nusselt no correlation for forced convection is given by[17]

$$Nu = 0.3 + \frac{0.62Re^{1/2}Pr^{1/3}}{\left[1+\left(\frac{0.4}{Pr}\right)^{2/3}\right]^{1/4}}\left[1+\left(\frac{Re}{282,000}\right)^{5/8}\right]^{4/5} = 707.1227321 \tag{3.8}$$

The corresponding value of the heat transfer coefficient is h_o = 8.881461515 W/m^2K.

3.1.6. Heat flux and retention time:

There is unsteady heat transfer taking place from the salt to the environment as the temperature of the salt as well as the heat flux is time-dependent. To quantify the heat flux and the time required for the temperature of the salt to reach its melting point, an analytical heat transfer model is developed.

System assumptions:

- The tank is insulated from top and bottom.
- Only one-dimensional heat transfer is considered.
- The initial temperature of the salt is 838K.
- The outside temperature of the air is 283K.

The following system of equations represents the transfer of heat from the salt to the ambient:

$$-m_{\text{ms}} \cdot cp_{\text{ms}} \cdot \frac{T_{\text{ms1}} - T_{\text{ms0}}}{\Delta t} = \frac{T_{\text{ms1}} - T_{\text{w1}}}{R_{\text{ms}} \cdot \left(\frac{1}{\text{area}}\right)} \tag{3.9}$$

$$\frac{T_{\text{ms1}} - T_{\text{w1}}}{R_{\text{ms}}} = \frac{T_{\text{w1}} - T_{\text{air}}}{R_{\text{air}}} \tag{3.10}$$

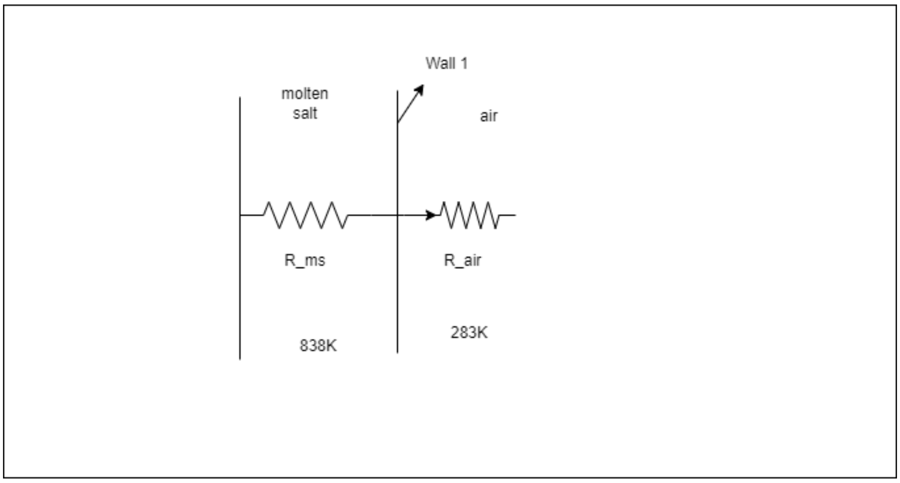

Figure 3.2: : Thermal resistance network

Constant parameters:
The list below contains the parameters which are constant with time for the above system of equations.

- m_{ms} = 16145.50714 kg
- cp_{ms} = 1596.46 J/kg.K
- $R_{ms} = 1/h_i$ = 0.00121482 m^2K/W
- area = 18.85793876 m^2
- Δt = 60s
- $R_{air} = 1/h_o$ = 0.103737411 m^2K/W

Equation (3.11) represents the heat released by the molten salt which is then absorbed by the wall. This heat is then further lost to the environment which is given by equation(3.14). An iterative simulation is performed in Matlab to find the values of T_{ms1} and T_{w1} and the time required for T_{ms0} to reach 519.3K.

3.2. Heat loss with PCM

To enhance the thermal insulation of the storage tank, we employ a PCM designed to absorb and store heat lost by the molten salt, thereby significantly reducing overall heat loss. The choice of PCM is crucial and must align with the system's operating temperature range, specifically between 519.3 K and 838 K. A PCM with a melting point slightly above that of the solar salt will not only facilitate phase transition but also serve as a thermal indicator, signaling that the temperature of the molten salt is nearing its melting point.

After evaluating the available PCMs, we have selected a composition predominantly based on **Lithium Chloride (LiCl)**, augmented with either Potassium Chloride (KCl) or Sodium Chloride (NaCl). The chosen PCM comprises 30-50% LiCl by mass, providing an optimal balance of thermal properties suitable for our system requirements.[23] The thermophysical properties of the PCM as listed in 3.2[13][22]:

Property	Unit	Value
Melting Point	[K]	626
Density	$[kg/m^3]$	2060
Specific Heat	$[J/kgK]$	1520
Thermal Conductivity	$[W/mK]$	0.56
Dynamic Viscosity	$[Pas]$	0.002
Latent heat of melting	$[J/kg]$	230000

3.2.1. Release of heat from PCM:

The PCM layer is designed with a thickness of 0.25 m, providing a conductive resistance calculated using Equation (3.7) to be 0.4464 m^2K/W. To determine whether heat is released or absorbed by this specific PCM layer thickness, a system of equations is formulated, accounting for the heat transfer through the PCM layer. This analysis is critical for understanding the thermal behavior and effectiveness of the PCM in reducing heat loss from the tank.

System assumptions:

- The tank is insulated from top and bottom and only 1D heat transfer is considered.
- The initial temperature of the salt is 838K and the outside air temperature is 283K.
- The initial temperature of PCM is 626K and it is completely in **liquid** phase.
- The mass of PCM required is 10915 kg.

$$-m_{\text{ms}} \cdot cp_{\text{ms}} \cdot \frac{T_{\text{ms1}} - T_{\text{ms0}}}{\Delta t} = \frac{T_{\text{ms1}} - T_{\text{w1}}}{R_{\text{ms}} \cdot \left(\frac{1}{\text{area}}\right)} \tag{3.11}$$

$$\frac{T_{\text{ms1}} - T_{\text{w1}}}{R_{\text{ms}} \left(\frac{1}{\text{area}_{ms}}\right)} = \frac{T_{\text{w1}} - T_{\text{pcm1}}}{R_{\text{pcm}} \left(\frac{1}{\text{area}_{pcm}}\right)} \tag{3.12}$$

$$-m_{\text{pcm}} cp_{\text{pcm}} \frac{T_{\text{pcm1}} - T_{\text{pcm0}}}{\Delta t} = \frac{T_{\text{w1}} - T_{\text{w2}}}{R_{\text{pcm}} \left(\frac{1}{\text{area}_{\text{pcm}}}\right)} - \frac{T_{\text{ms1}} - T_{\text{w1}}}{R_{\text{ms}} \left(\frac{1}{\text{area}_{ms}}\right)} \tag{3.13}$$

$$\frac{T_{\text{w1}} - T_{\text{w2}}}{R_{\text{pcm}}} = \frac{T_{\text{w2}} - T_{\text{air}}}{R_{\text{air}}} \tag{3.14}$$

The above equations confirm the release of heat by the PCM layer for a thickness of 0.25m.(3.13) accounts for the heat released by the PCM with the negative sign on the left-hand side term indicating the release of heat. Hence, we go ahead with the considered thickness.

3.2.2. Heat loss through PCM:

Once we confirm the release of heat through the PCM, our next step involves modeling the system to comprehensively analyze heat transfer dynamics, encompassing both conduction through the PCM and the phase change process. In this phase, our focus shifts to calculating the time required for the molten salt to reach its melting point, considering the thermal effects of PCM phase change throughout this duration. This analysis is crucial for understanding the intricate interplay between thermal conductivity, phase transition, and overall system efficiency in thermal storage applications.

The assumptions and constant parameters established in the previous heat release analysis remain unchanged for our current model. This advanced model incorporates two distinct sets of equations to describe heat transfer phenomena. The first set addresses heat transfer while the PCM exists in both liquid and solid phases, capturing the dynamic phase transition process. The second set pertains to single-phase heat transfer occurring after the complete solidification of the PCM. This thermal resistance model helps in understanding and analyzing the heat transfer mechanism through the molten salt and PCM, considering both liquid and solid phases of the PCM. It is essential for calculating the time required for the molten salt to reach its melting point and for optimizing the thermal insulation properties of the system. The resistances of liquid and solid phases of PCM are variable as the thickness of these layers is dependent on time and is given by:

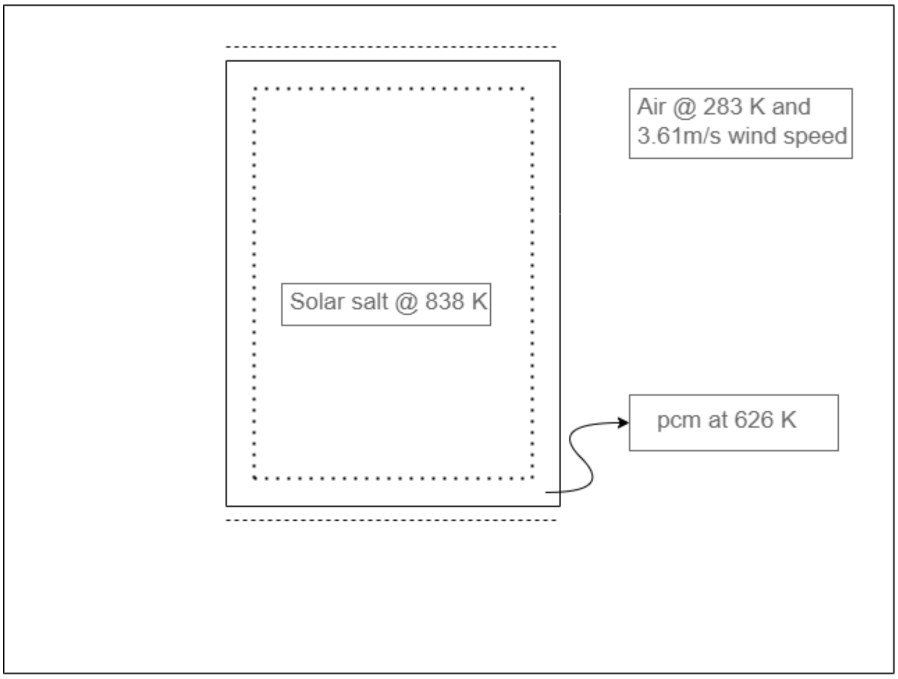

Figure 3.3: Molten salt storage tank with PCM insulation

$$R_{\text{liq\_pcm}} = \frac{0.25\left(\frac{m_{\text{liq\_pcm1}}}{m_{\text{pcm}}}\right)}{k_{\text{pcm}}} \quad (3.15)$$

$$R_{\text{sol\_pcm}} = \frac{0.25\left(\frac{m_{\text{sol\_pcm1}}}{m_{\text{pcm}}}\right)}{k_{\text{pcm}}} \quad (3.16)$$

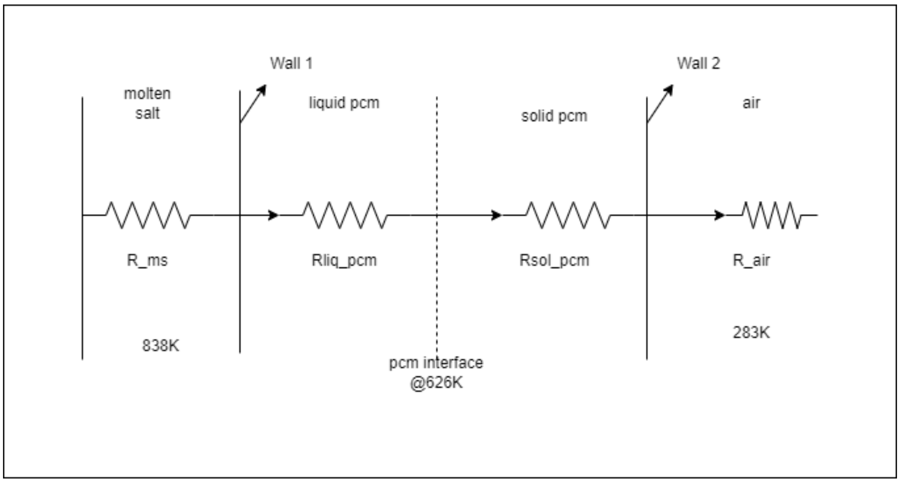

Figure 3.4: Thermal resistance network of PCM model

These expressions for the resistances are then used in the system of our heat transfer equations. [12]

$$-m_{\text{ms}} \cdot cp_{\text{ms}} \cdot \frac{T_{\text{ms1}} - T_{\text{ms0}}}{\Delta t} = \frac{T_{\text{ms1}} - T_{\text{w1}}}{R_{\text{ms}} \cdot \left(\frac{1}{\text{area}}\right)} \tag{3.17}$$

$$\frac{T_{\text{ms1}} - T_{\text{w1}}}{R_{ms}\left(\frac{1}{\text{area}}\right)} = \frac{T_{\text{w1}} - T_{\text{pcm}}}{\left(\frac{0.25\left(\frac{m_{\text{liq\_pcm1}}}{m_{\text{pcm}}}\right)}{k_{\text{pcm}}}\right)\left(\frac{1}{\text{area}}\right)} \tag{3.18}$$

$$\frac{(m_{\text{sol\_pcm1}} - m_{\text{sol\_pcm0}})h_f}{\Delta t} = \frac{T_{\text{pcm}} - T_{\text{w2}}}{\left(\frac{0.25\left(\frac{m_{\text{sol\_pcm1}}}{m_{\text{pcm}}}\right)}{k_{\text{pcm}}}\right)\left(\frac{1}{\text{area}}\right)} - \frac{T_{\text{w1}} - T_{\text{pcm}}}{\left(\frac{0.25\left(\frac{m_{\text{liq\_pcm1}}}{m_{\text{pcm}}}\right)}{k_{\text{pcm}}}\right)\left(\frac{1}{\text{area}}\right)} \tag{3.19}$$

$$\frac{T_{\text{pcm}} - T_{\text{w2}}}{0.25\left(\frac{m_{\text{sol\_pcm1}}}{m_{\text{pcm}}}\right)/k_{\text{pcm}}} = \frac{T_{\text{w2}} - T_{\text{air}}}{R_{\text{air}}} \tag{3.20}$$

$$m_{\text{pcm}} = m_{\text{liq\_pcm1}} + m_{\text{sol\_pcm1}} \tag{3.21}$$

This set of equations addresses the transfer of heat taking place when the PCM is in both solid and liquid phases. Eqn (3.19) accounts for the latent heat stored in the solid mass of the PCM forming at every time step which is equal to the difference of the heat fluxes between the solid and liquid parts of the PCM. Loss of sensible heat through liquid and solid phases is ignored as it is considered to be negligible as compared to the latent heat. Eqns (3.18) & (3.20) give the wall fluxes on either side of the PCM interface and the temperature of the PCM is considered to be constant at 626K. Eqn (3.21) gives the mass balance of the PCM layer. After complete solidification of the PCM layer, only sensible heat transfer will take place in the system which is given by the following system of equations:

$$-m_{\text{ms}} \cdot cp_{\text{ms}} \cdot \frac{T_{\text{ms1}} - T_{\text{ms0}}}{\Delta t} = \frac{T_{\text{ms1}} - T_{\text{w1}}}{R_{\text{ms}} \cdot \left(\frac{1}{\text{area}}\right)} \tag{3.22}$$

$$\frac{T_{\text{ms1}} - T_{\text{w1}}}{R_{\text{ms}}\left(\frac{1}{\text{area}_{ms}}\right)} = \frac{T_{\text{w1}} - T_{\text{pcm1}}}{R_{\text{pcm}}\left(\frac{1}{\text{area}_{pcm}}\right)} \tag{3.23}$$

$$-m_{\text{pcm}} cp_{\text{pcm}} \frac{T_{\text{pcm1}} - T_{\text{pcm0}}}{\Delta t} = \frac{T_{w1} - T_{w2}}{R_{\text{pcm}}\left(\frac{1}{\text{area}_{\text{pcm}}}\right)} - \frac{T_{ms1} - T_{w1}}{R_{ms}\left(\frac{1}{\text{area}_{ms}}\right)} \tag{3.24}$$

$$\frac{T_{\text{w1}} - T_{\text{w2}}}{R_{\text{pcm}}} = \frac{T_{\text{w2}} - T_{\text{air}}}{R_{\text{air}}} \tag{3.25}$$

In this system, the entire mass of PCM layer exists in the solid phase, and hence there is a constant resistance value for the PCM. Eqn (3.24) gives the sensible heat released from the PCM layer along with the wall heat fluxes given by eqns (3.23) & (3.25)

3.3. Ansys Validation

A second method of analyzing the heat loss through the system is also considered. CFD simulations are performed to analyze the heat transfer through the PCM and the change in retention time of the molten salt. This analysis is done in Ansys Fluent. It is a computational fluid dynamics (CFD) software package widely used for simulating fluid flow, heat transfer, and related phenomena. It offers a wide range of models to simulate complex physical phenomena such as turbulence, combustion, multiphase flows, and conjugate heat transfer. This makes it suitable for a diverse range of applications in engineering and research. Fluent employs robust solvers that are capable of handling both steady-state and transient simulations. It supports various numerical methods and algorithms to solve fluid dynamics and heat transfer equations accurately. It also supports customization through user-defined functions (UDFs) for specialized applications.

3.3.1. Problem Analysis:

The analysis is conducted for three types of systems:

1. molten salt tank with no insulation.
2. PCM solidification time.
3. molten salt tank with PCM insulation.

The problem is an unsteady heat transfer problem based on natural convection, conduction, and forced convection.

3.3.2. Methodology:

Fig 3.5 shows the steps taken while approaching the problem.

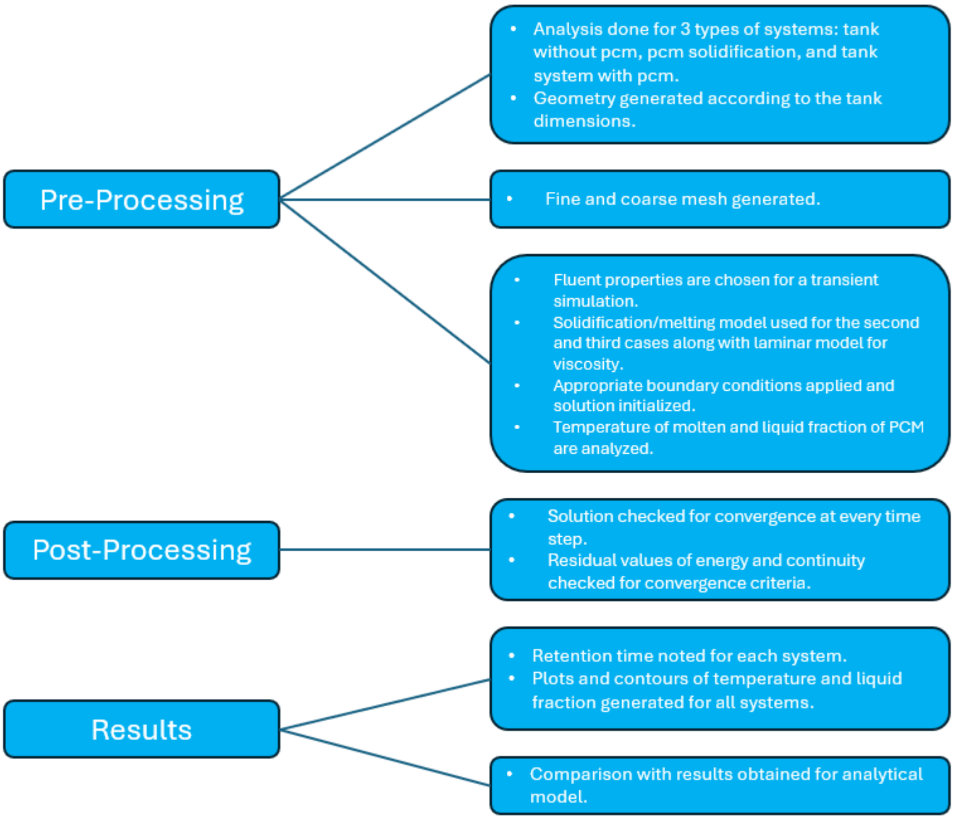

- Analysis done for 3 types of systems: tank without pcm, pcm solidification, and tank system with pcm.
- Geometry generated according to the tank dimensions.

- Fine and coarse mesh generated.

- Fluent properties are chosen for a transient simulation.
- Solidification/melting model used for the second and third cases along with laminar model for viscosity.
- Appropriate boundary conditions applied and solution initialized.
- Temperature of molten and liquid fraction of PCM are analyzed.

- Solution checked for convergence at every time step.
- Residual values of energy and continuity checked for convergence criteria.

- Retention time noted for each system.
- Plots and contours of temperature and liquid fraction generated for all systems.

- Comparison with results obtained for analytical model.

Figure 3.5: Steps followed for CFD simulation

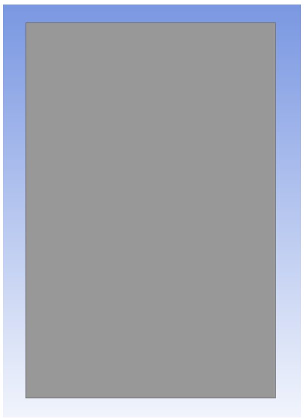

Figure 3.6: Geometry without PCM

3.3.3. Molten salt tank with no insulation:

Initially, we considered the molten salt tank without any insulation to analyze the temperature variation and retention time for the salt. Fig **??** & **??** show the geometry and mesh of the tank. The same tank dimensions as in the analytical model are considered. The quality of the mesh significantly impacts the accuracy and efficiency of the simulation results. In this simulation project, we opted for a structured mesh comprised of quadrilateral elements, as the geometry exhibits relatively simple characteristics. This choice of mesh type facilitates efficient simulation of the flow dynamics while maintaining a high level of accuracy. Edge size meshing is done for the tank edges based on the number of divisions having **180** and **270** divisions for shorter and longer edges respectively. Along with this, face meshing with an element size of **0.1984m** is done for a uniform mesh. The edges of the tank are named salt side, top, ambient, and bottom.

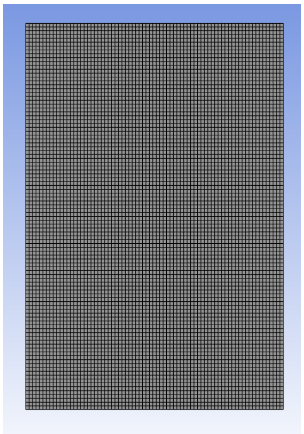

Figure 3.7: Mesh without PCM

Setup and Solution:

The simulations were performed with a transient pressure-based solver along with the gravity effects. Laminar viscous model was used as it accurately captures the fluid dynamics in such cases, ensuring the simulation is representative of the actual physical behavior. It is less complex than turbulent models, leading to reduced computational

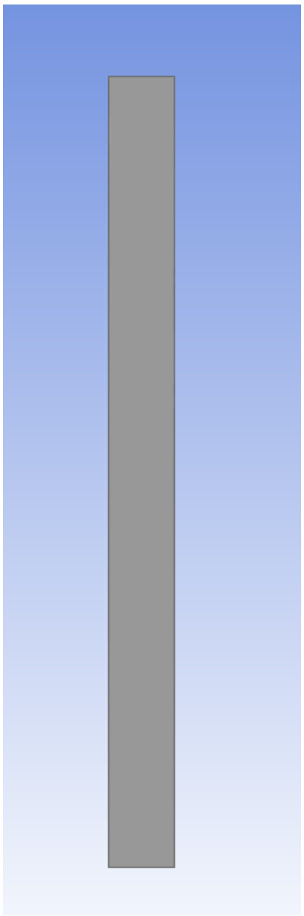

Figure 3.8: Geometry PCM

requirements and simpler implementation. It also effectively handles the boundary layer development in natural convection-dominated scenarios. The material properties of solar salt are input and then wall boundary conditions are given for salt side and ambient having constant temperatures of **838K** & **283K** respectively. The top and bottom walls are given zero heat flux boundary conditions as they are considered insulated. The convergence criteria for the energy residual is 10^{-6} and that for the continuity residual is 10^{-3}. The solution is checked for convergence at every time step. The solution method used is Second order upwind as it improves the accuracy of the simulation by reducing numerical diffusion and capturing sharper gradients in the solution. The solution is simulated with a time step size of **1s** for 40 hours. The temperature of solar salt is plotted with time and the results are compared with the analytical model.

3.3.4. PCM Solidification:

Simulations were performed separately only on the PCM layer to analyze the solidification time and the liquid fraction of the PCM.The thickness of the PCM layer is 0.25m. The type of meshing remains the same as done for the earlier case.

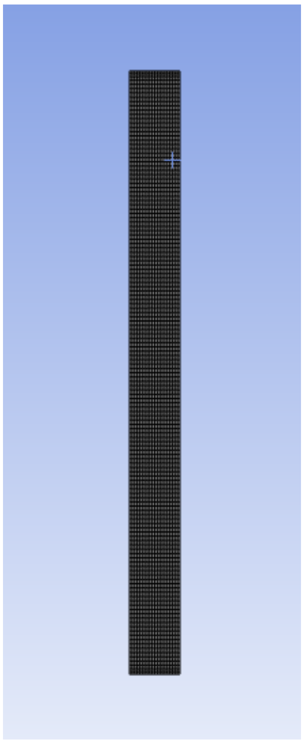

Figure 3.9: Mesh PCM

3.3.5. Numerical Methodology:

The numerical approach, in the current investigation, uses the enthalpy-porosity method to predict the transient behavior of the PCM. In this technique, the melt interface is not tracked explicitly. Instead, a quantity called the liquid fraction, which indicates the fraction of the cell volume that is in liquid form, is associated with each cell in the domain. The liquid fraction is computed at each iteration, based on an enthalpy balance. The mushy zone is a region in which the liquid fraction lies between 0 and 1. The mushy zone is modeled as a ”pseudo” porous medium in which the porosity decreases from 1 to 0 as the material solidifies. When the material has fully solidified in a cell, the porosity becomes zero and hence the velocities also drop to zero.[6] [2]

Energy Equations:

The enthalpy of the material is computed as the sum of the sensible enthalpy, h, and the latent heat, ΔH:[6][2]

$$H = h + \Delta H \tag{3.26}$$

where

$$h = h_{\text{ref}} + \int_{T_{\text{ref}}}^{T} c_p dT$$

(3.27)

and

h_{ref} = reference enthalpy
T_{ref} = reference temperature
c_p = specific heat at constant pressure

The liquid fraction, β, can be defined as[6]

$$\beta = 0 \text{ if } T < T_{\mathrm{solidus}}$$
$$\beta = 1 \text{ if } T > T_{\mathrm{liquidus}}$$
$$\beta = \frac{T - T_{\mathrm{solidus}}}{T_{\mathrm{liquidus}} - T_{\mathrm{solidus}}} \text{ if } T_{\mathrm{solidus}} < T < T_{\mathrm{liquidus}}$$

The latent heat content can now be written in terms of the latent heat of the material, L[6]:

$$\Delta H = \beta L \tag{3.28}$$

For solidification/melting problems, the energy equation is written as[6]:

$$\frac{\partial}{\partial t}(\rho H) + \nabla \cdot (\rho \vec{v} H) = \nabla \cdot (k \nabla T) + S \tag{3.29}$$

where

H = enthalpy (eq3.26)
ρ = density
$\vec{v}$ = fluid velocity
S = source term

Momentum Equations:
The enthalpy porosity model accounts for the fluid flow in the liquid phase and incorporates the effects of the solid phase by introducing a source term that models the resistance to flow in regions where the material is solidifying.[6][27]

Continuity equation

$$\frac{\partial \rho}{\partial t} + \nabla \cdot (\rho \mathbf{u}) = 0 \tag{3.30}$$

Conservation of momentum

$$\frac{\partial}{\partial t}(\rho \mathbf{u}) + \nabla \cdot (\rho \mathbf{u}\mathbf{u}) = -\nabla p + \nabla \cdot (\mu \nabla \mathbf{u}) + \mathbf{S} \tag{3.31}$$

The source term, S is given by

$$S = \frac{(1-\beta)^2}{(\beta^3 + \epsilon)} A_{\mathrm{mush}} (\vec{v} - \vec{v}_p) \tag{3.32}$$

where β is the liquid volume fraction, ϵ is a small number (0.001) to prevent division by zero, A_{mush} is the mushy zone constant, and $\vec{v}_p$ is the solid velocity due to the pulling of solidified material out of the domain (also referred to as the pull velocity).

Setup and Solution:
The simulations were performed with a transient pressure-based solver along with the gravity effects. The Laminar viscous model was used as it accurately captures the fluid dynamics in such cases, ensuring the simulation is representative of the actual physical behavior. The Solidification/Melting model is used to accurately model the phase change of the PCM. The mushy zone parameter for this model is 10000. The solidification enables the user to input the solidus and liquidus temperature of the PCM which is input as 626K, the melting point of our PCM. The wall boundary condition for the salt side is a constant temperature boundary condition at 838K and that for the ambient wall is 283K. The convergence criteria for the energy residual is 10^{-6} and that for the continuity residual is 10^{-3}. The solution is checked for convergence at every time step. The solution method used is First order upwind. The solution is initialized at the temperature of 627K to ensure that the PCM is in a completely liquid state. The solution is simulated with a time step size of **1s** until the PCM is completely solidified.

3.3.6. Molten salt tank with PCM insulation:

In this case, we simulated the entire tank system to analyze the retention time, check the increase in the retention time with and without the PCM insulation, and compare the results with the analytical model. A wall of thickness 0.01 m separates both the fluids in the geometry. The type of meshing remains the same as done for the earlier case. A finer mesh is created to obtain convergence and accurate results.

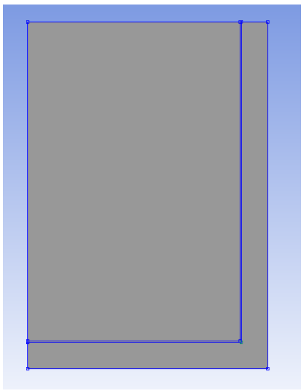

Figure 3.10: Geometry of entire model

Mesh Dependency:
Three different meshes are generated for the model consisting of 20000, 70000 and 90000 elements. No significant differences were noticed between the meshes having 70000 and 90000 elements. Hence, for faster computation time, the mesh with 70000 elements is selected. Although the geometry of the problem is 2 dimensional, the CPU time of the simulations is very high due to the slow solidification process of the PCM.

Setup and Solution:
The simulations were performed with a transient pressure-based solver along with the gravity effects. The Laminar viscous model was used as it accurately captures the

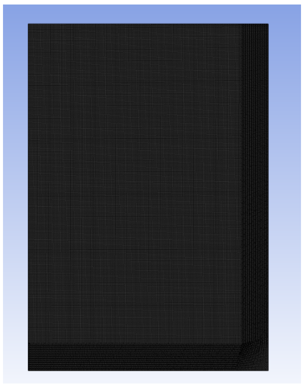

Figure 3.11: Mesh of entire model

fluid dynamics in such cases, ensuring the simulation is representative of the actual physical behavior. The Solidification/Melting model is used to accurately model the phase change of the PCM. The mushy zone parameter for this model is 10000. The solidification enables the user to input the solidus and liquidus temperature of the PCM which is input as 626K, the melting point of our PCM. The wall boundary condition for the salt side is a constant temperature boundary condition at 838K and that for the ambient wall is 283K. A coupled boundary condition is given for the wall separating solar salt and the PCM. The convergence criteria for the energy residual is 10^{-6} and that for the continuity residual is 10^{-3}. The solution is checked for convergence at every time step. The solution method used is First order upwind. The solution is initialized at the temperature of 838 K for all zones. The PCM interior temperature is given by a patch at 627 K. The solution is simulated with a time step size of **1s**.

4

Results

As discussed in chapter 3, first an analytical heat transfer model was built using necessary heat transfer equations and it was analyzed for the three cases. The time required for the molten salt at 838 K to reach its melting point was simulated with and without the PCM insulation and the PCM solidification process was also analyzed. The same system is then simulated in Ansys Fluent to validate the analytical system outcomes.

4.1. Analytical Model Results

The analytical model comprising of heat transfer equations was simulated in Matlab for three scenarios.

4.1.1. Heat loss without PCM:

This system consisted of a molten salt storage tank and the heat loss from the tank was simulated to find the retention time of the molten salt and the heat flux from the storage tank. Fig 4.1 shows the change in temperature of molten salt with time. The time required for the initial temperature (838K) of the molten salt to reach its melting temperature (519.3 K) is **34 hours**. Fig 4.2 shows the heat flux from the molten salt with time. As the system is unsteady, the heat flux decreases with time. The maximum heat flux at t=0 is 5250 W/m^2 and the minimum heat flux at the last time step is 2250 W/m^2.

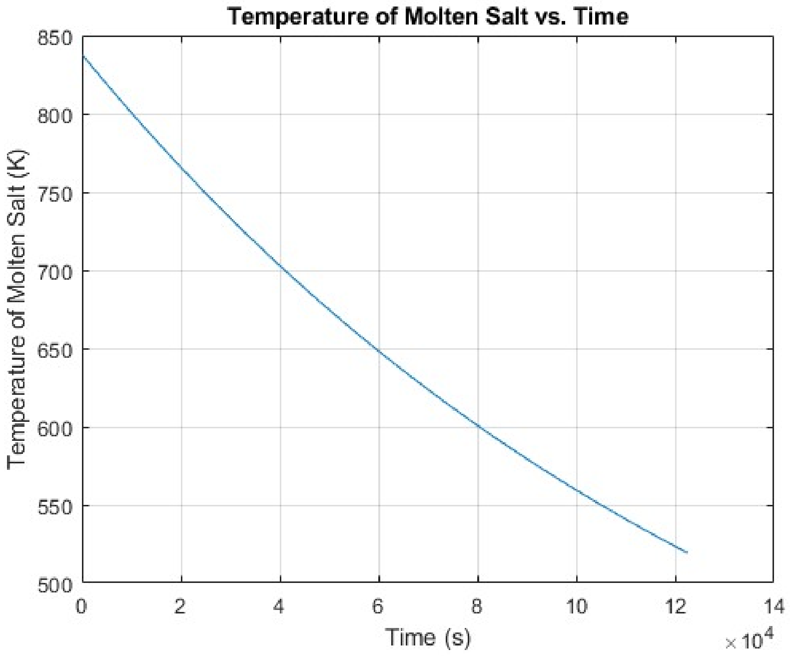

Figure 4.1: Temperature of molten salt without PCM

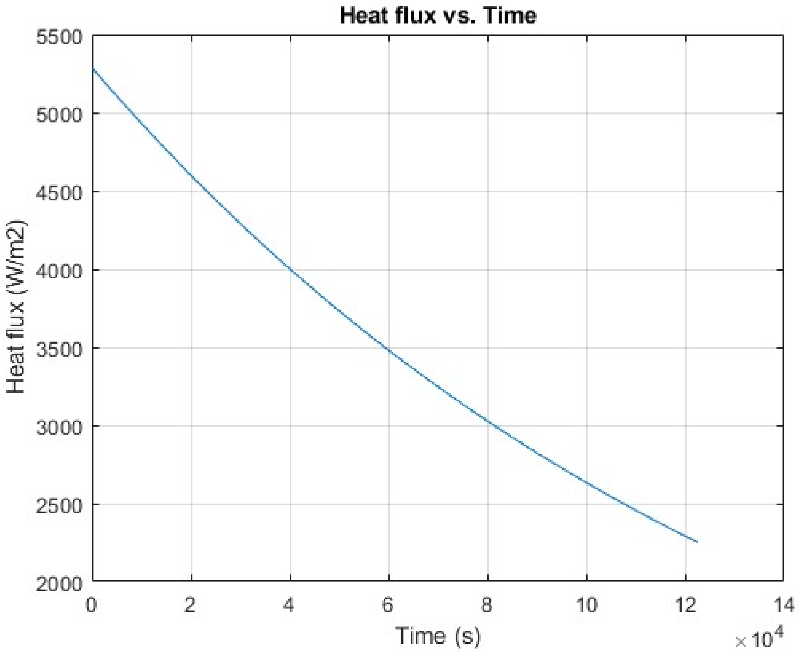

Figure 4.2: Heat flux without PCM

4.1.2. PCM Solidification:

In this case, the solidification process of the PCM was simulated to analyze its liquid fraction and solidification time.The time taken by the PCM to complete solidification is **128 hours** which is approximately 5 days.

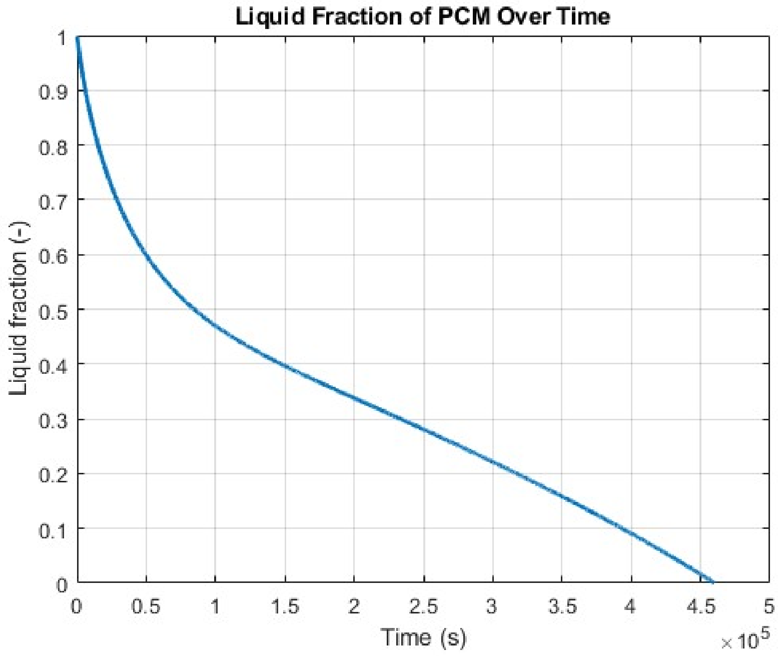

Figure 4.3: Liquid fraction of PCM

4.1.3. Heat Loss with PCM:

Here, the system was modeled to analyze the change in retention time of the molten salt after PCM insulation and the change in temperature of the molten salt. The time required for the temperature of molten salt to reach its melting point is **308 hours** which is close to 13 days.

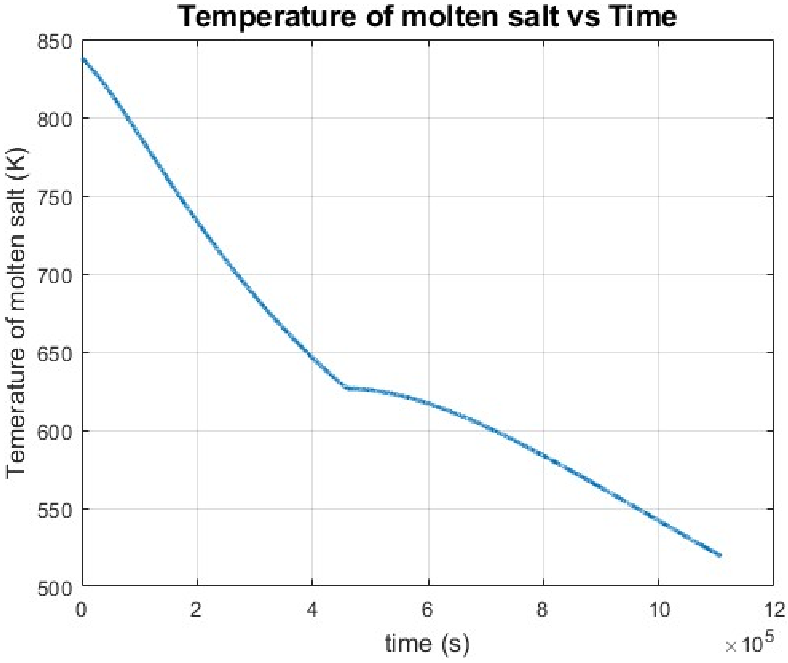

Figure 4.4: Temperature of molten salt with PCM insulation

4.2. Ansys Fluent Simulation Results:

CFD simulations were performed on the same case studies as in the analytical model to validate the results of that model.

The plots show the behavior of the temperature of molten salt with time. The time required to reach the melting temperature of molten is 37 hours according to the Fluent results which is slightly higher than the analytical model.

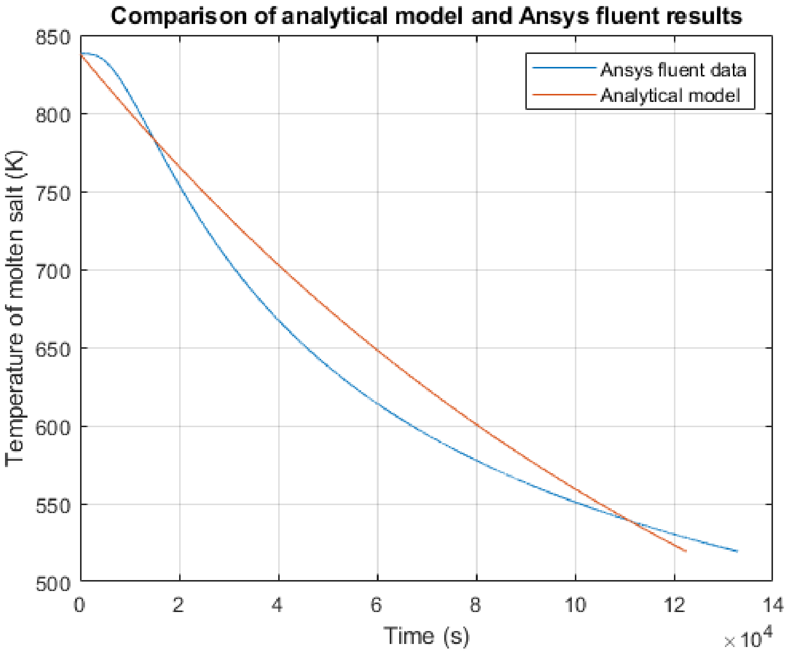

Figure 4.5: Temperature of molten salt without PCM

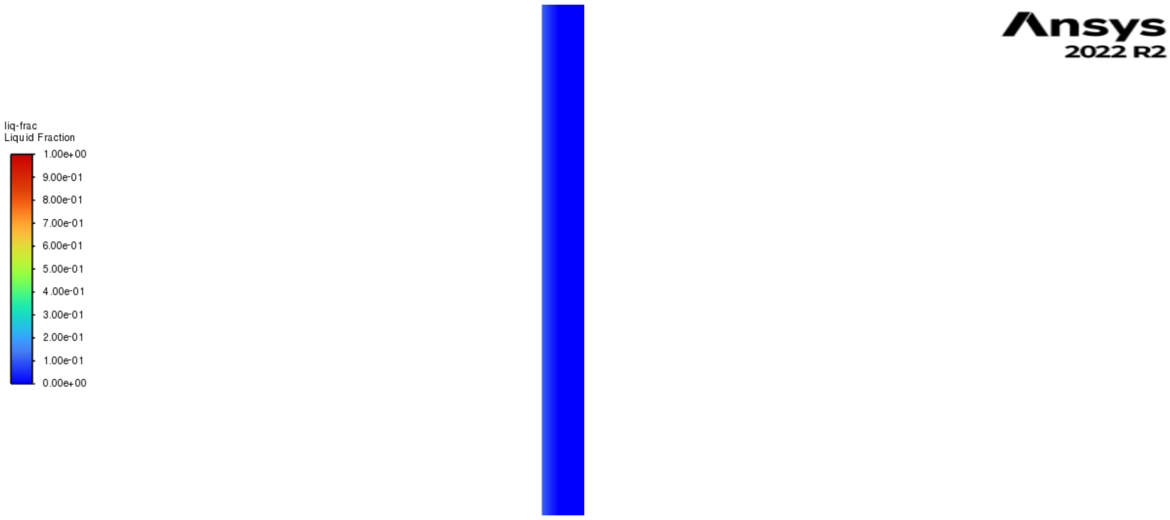

Figure 4.6: Liquid fraction of PCM

The contours represent the liquid fraction and temperature variation within the PCM layer after completely solidifying it. The entire PCM layer is at its melting temperature except for a small part close to the ambient side wall.

Figure 4.7: Temperature of PCM

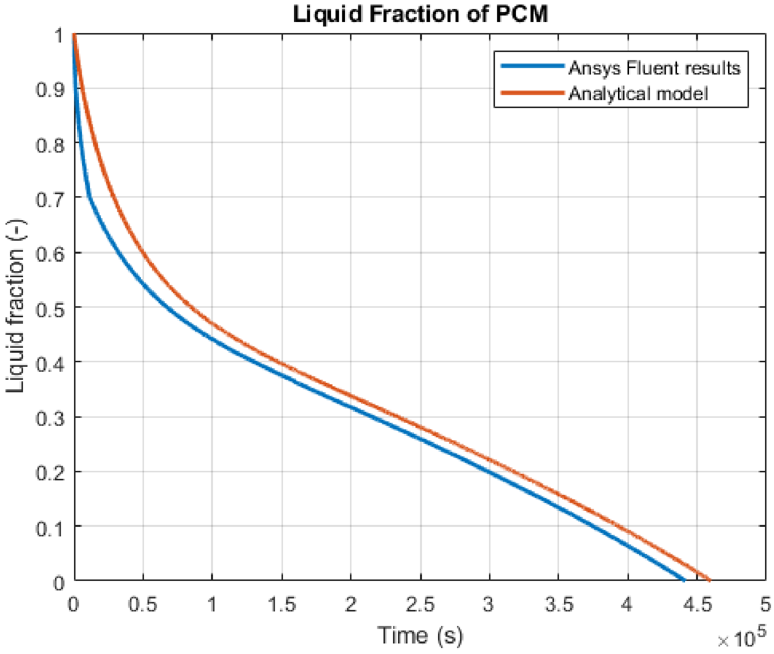

Figure 4.8: Liquid fraction of PCM

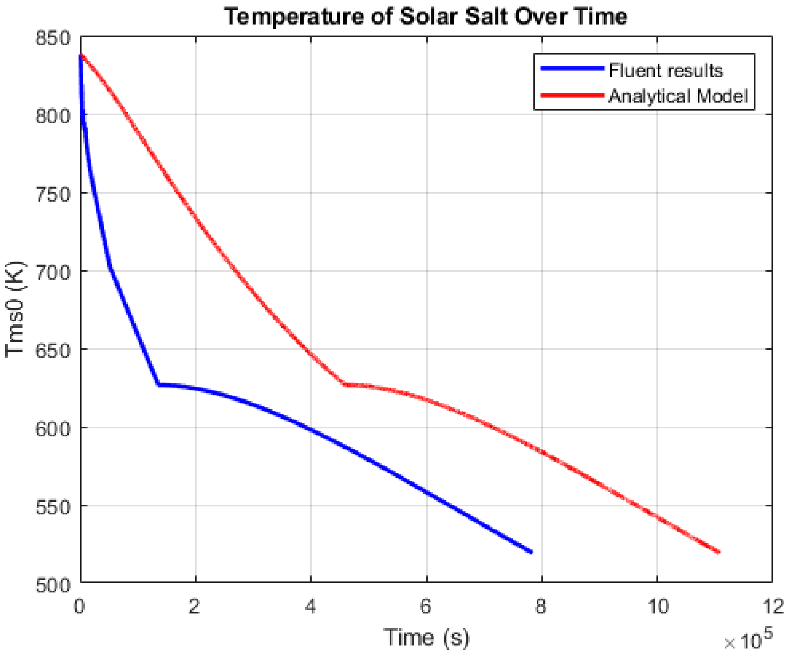

Figure 4.9: Temperature of molten salt with PCM insulation

The plots in fig 4.9 show the comparison of the Ansys fluent results with the analytical model for the variation of molten salt temperature with time. There is a substantial difference in the time the molten salt takes to reach its melting point in both cases. The solidification process of the PCM is faster in Fluent results as the PCM gets completely solidified in 38 hours. This difference can be attributed to the approximations made in the analytical model which could have resulted in a longer retention time. The time taken after the solidification is approximately the same in both cases which further validates the the claim of errors due to approximation made in the analytical model. The total time for the molten salt to reach its melting point is nearly 13 days for the analytical model and 9 days according to the Fluent results.

4.3. Sensitivity Analysis:

A sensitivity analysis was performed with the analytical model to study the change in the retention time of the molten salt with the change in the melting point of the PCM. The plots indicate that with the PCM having a melting point equal to 726K takes the longest for the temperature of molten salt to reach its melting temperature.

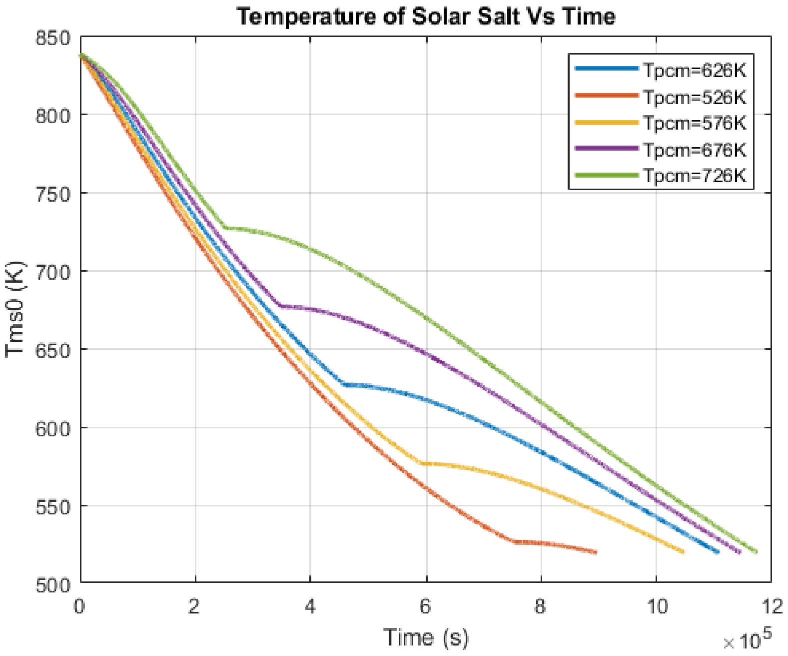

Figure 4.10: Temperature of molten salt with PCMs having different melting points

4.4. Cost Analysis:

While the use of PCM as an insulation is a sustainable method, a cost analysis is also done to compare the cost of PCM with the cost of external electrical heating. The use of PCM does not eliminate the use of external heaters, but only minimizes the dependency on it.

We consider that the heating is started once the temperature of the molten salt reaches 600K. The energy required for this temperature difference is given by

$$Q = mc_p\Delta T = 1703.5kWh \tag{4.1}$$

Assuming that our heater takes 8 hours to fully charge the tank, the capacity of the heater required is

$$P = \frac{1703.5}{8} = 213kW \tag{4.2}$$

4.4.1. System without any insulation:

For the system without any insulation, it takes 22 hours for the initial temperature of molten salt to drop to 600K. The average cost of electricity in the Netherlands for industrial use is 0.25 euros/kWh.[24] Hence, the cost required to charge the system once is 424 euros. Further, the annual cost of heating is

Annual cost = $\frac{424*8760}{30}$ = 123,808 euros

4.4.2. System with PCM insulation:

For the system with PCM as an insulation, it takes 198 hours for the initial temperature of molten salt to drop to 600K. The mass of PCM required is 10915 kg. The annual cost of heating becomes

$$\text{Annual cost} = \frac{424*8760}{116} = 32019 \text{ euros}$$

The cost of PCM is 15 euros/kg. Hence, the total cost of PCM is 163725 euros. The average lifespan of PCM is 5 years. Hence, the annual cost of PCM is 32745 euros. Additional shipping and import costs in the range of 5000-7000 euros will also be incurred.

Considering all other miscellaneous costs, the total cost is

$$\text{Annual cost} = 32019 + 32745 + 70000 + 12000 = 83{,}764 \text{ euros}$$

5

Conclusion

The study investigated various high-temperature thermal energy storage (TES) technologies, focusing particularly on the use of phase change materials (PCM) as an insulation medium to reduce heat loss in molten salt tanks. An inorganic LiCl-based PCM was selected for this purpose. An analytical model was developed and simulated in Matlab to examine three specific scenarios, and these results were cross-validated with computational fluid dynamics (CFD) simulations conducted using ANSYS Fluent. The findings revealed that incorporating a 0.25m thick layer of PCM significantly increased the retention time of the molten salt storage tank from 34 hours without insulation to 216 hours. Furthermore, a cost comparison indicated that the PCM-based system was approximately 40,000 euros cheaper than systems utilizing electrical heaters. Thus, this research highlights that using PCM not only offers a sustainable and efficient method for heat retention but also proves to be economically advantageous.

5.1. Further Scope and Recommendations:

- These results can be further verified by conducting experiments that will give more accurate and real-life results.
- There is considerable difference between the results of the analytical model and Fluent results for the PCM solidification time. Incorporating the sensible heat loss terms for the solid and liquid layers of the PCM will lead to more accurate results.
- Only 1-dimensional heat transfer was considered in the analytical model and a uniform temperature was assumed for the molten salt tank. Hence, the results will vary with the experimental results.
- The property data for molten salts and PCMs is highly confidential and not disclosed by the industries. Hence, approximate values were used. Collaborating with a PCM manufacturing industry for this research can provide more accurate results.
- Different kinds of PCM can be used as insulation and investigated further.

- The implementation of this alternative can be quite complex, hence starting with a prototype plant can be a good option.
- The dimensions of the tank and the thickness of the PCM layer can be altered acoording to the requirement.

References

[1] E Z A R Z A M Oya and Ciemat -Plataforma Solar de Almería. *7 Parabolic-trough concentrating solar power (CSP) systems*. Tech. rep.

[2] Mohamed Ali, Ahmed K. Alkaabi, and Jeong Ik Lee. "CFD simulation of an integrated PCM-based thermal energy storage within a nuclear power plant connected to a grid with constant or variable power demand". In: *Nuclear Engineering and Design* 394 (Aug. 2022). ISSN: 00295493. DOI: `10.1016/j.nucengdes.2022.111819`.

[3] Ryan Anderson et al. "Experimental results and modeling of energy storage and recovery in a packed bed of alumina particles". In: *Applied Energy* 119 (Apr. 2014), pp. 521–529. ISSN: 03062619. DOI: `10.1016/j.apenergy.2014.01.030`.

[4] Ryan Anderson et al. "Packed bed thermal energy storage: A simplified experimentally validated model". In: *Journal of Energy Storage* 4 (Dec. 2015), pp. 14–23. ISSN: 2352152X. DOI: `10.1016/j.est.2015.08.007`.

[5] "Annual Wind Speed Averages for the Netherlands - Current Results". In: ().

[6] "ANSYS FLUENT 12.0 Theory Guide - 17. Solidification and Melting". In: ().

[7] Mohammad M.S. Al-Azawii et al. "Experimental study on packed-bed thermal energy storage using recycled ceramic as filler materials". In: *Journal of Energy Storage* 44 (Dec. 2021). ISSN: 2352152X. DOI: `10.1016/j.est.2021.103375`.

[8] Alexander Bonk and Thomas Bauer. *Solar Salt-Thermal Property Analysis Report on thermo-physical properties of binary NaNO 3-KNO 3 mixtures in a range of 59-61 wt% NaNO 3*. Tech. rep.

[9] "download". In: ().

[10] Jacob Edwards and Hitesh Bindra. "An experimental study on storing thermal energy in packed beds with saturated steam as heat transfer fluid". In: *Solar Energy* 157 (2017), pp. 456–461. ISSN: 0038092X. DOI: `10.1016/j.solener.2017.08.065`.

[11] Judith C Gomez. *High-Temperature Phase Change Materials (PCM) Candidates for Thermal Energy Storage (TES) Applications*. Tech. rep. 2011. URL: `http://www.osti.gov/bridge`.

[12] S.C. Gupta. "The Stefan Problem and Its Classical Formulation". In: *The Classical Stefan Problem*. Elsevier, 2018, pp. 1–35. DOI: `10.1016/b978-0-444-63581-5.00001-4`.

[13] "H Range Study". In: ().

[14] Michel Y. Haller et al. “Methods to determine stratification efficiency of thermal energy storage processes - Review and theoretical comparison”. In: *Solar Energy* 83.10 (Oct. 2009), pp. 1847–1860. ISSN: 0038092X. DOI: `10.1016/j.solener.2009.06.019`.

[15] K A R Ismail and R Stuginsky. *A parametric study on possible ®xed bed models for pcm and sensible heat storage*. Tech. rep.

[16] A Mathur et al. *For SolarPACES 2013 USING ENCAPSULATED PHASE CHANGE SALTS FOR CONCENTRATED SOLAR POWER PLANT*. Tech. rep.

[17] Anthony F. Mills and Carlos F.M. Coimbra. *Basic heat and mass transfer*. Prentice Hall, 2015, p. 1001. ISBN: 9780996305303.

[18] *Molten salt energy storage Ensuring the reliability of renewable power generation with superior time flexibility*. Tech. rep.

[19] “Netherlands - Climatology _ Climate Change Knowledge Portal”. In: ().

[20] Takahiro Nomura et al. “Microencapsulation of Metal-based Phase Change Material for High-temperature Thermal Energy Storage”. In: *Scientific Reports* 5 (Mar. 2015). ISSN: 20452322. DOI: `10.1038/srep09117`.

[21] A. Pasupathy, R. Velraj, and R. V. Seeniraj. *Phase change material-based building architecture for thermal management in residential and commercial establishments*. Jan. 2008. DOI: `10.1016/j.rser.2006.05.010`.

[22] “PlusICE H355 DSC”. In: ().

[23] “PlusICE H355 MSDS”. In: ().

[24] “Prices of natural gas and electricity _ CBS”. In: ().

[25] C. C.. Sorrell, Sunao. Sugihara, and Janusz. Nowotny. *Materials for energy conversion devices*. Woodhead, 2005, p. 416. ISBN: 9781855739321.

[26] *Thermal Energy Storage Technologies for Sustainability Thermochemical Energy Storage 6.1 INTRODUCTION*. Tech. rep. 2014.

[27] V R Voller and C Prakash. *A fixed grid numerical mode ing methodology for convection-diffusion mushy region phase-change problems*. Tech. rep. 1987, pp. 1709–1719.

[28] R. Weber and V. Dorer. “Long-term heat storage with NaOH”. In: *Vacuum* 82.7 (Mar. 2008), pp. 708–716. ISSN: 0042207X. DOI: `10.1016/j.vacuum.2007.10.018`.

[29] Tianyu Yang, William P. King, and Nenad Miljkovic. *Phase change material-based thermal energy storage*. Aug. 2021. DOI: `10.1016/j.xcrp.2021.100540`.

[30] Xin Zhou et al. “Encapsulated Copper-Based Phase-Change Materials for High-Temperature Heat Storage”. In: *ACS Omega* 7.6 (Feb. 2022), pp. 5442–5452. ISSN: 24701343. DOI: `10.1021/acsomega.1c06751`.

6

Appendix

6.1. Matlab Code:

6.1.1. Heat loss without PCM

Listing 6.1: Heat loss without PCM

```
clear all
clc
% Heat loss without any insulation or pcm
% Constant values
m = 16145.50714; % mass of solar salt in the tank (kg)
cp = 1596.46; % specific heat capacity of solar salt (J/kg.K)
Tms = 838; % intial temperature of the salt (K)
Rms =   0.00121482; % resistance of solar salt (W/m2K)
Rair = 0.103737411; % resistance of air (W/m2K)
area = 18.85793876; % cross-section area of the tank (m2)
Tair = 283; % ambient temperaute (K)
target_temp = 519.3; % melting point of solar salt (K)
delta_t = 60;%60; % time interval (seconds)

syms Tms1_sym Tw1_sym;
time = [];
Tms0_values = [];
q_values = [];
% Initalize variables
Tms0 = Tms;
t = 0;
while Tms0 > target_temp
  eq1 = -m*cp*(Tms1_sym-Tms0)/delta_t == (Tms1_sym - Tw1_sym)/(Rms*(1/area
     )); % heat loss equations
  eq2 = (Tms1_sym - Tw1_sym)/Rms == (Tw1_sym-Tair)/Rair;
  sol = vpasolve([eq1, eq2], [Tms1_sym, Tw1_sym]);
  Tms1_new = double(sol.Tms1_sym);
  Tw1_new = double(sol.Tw1_sym);

  % Update variables
  Tms0= Tms1_new;
  t = t + delta_t;
  q =(Tms1_new - Tair) / (Rair + Rms);
```

```
  time = [time, t];  % Append the current time
  Tms0_values = [Tms0_values, Tms0];  % Append the current temperature
  q_values = [q_values, q];
  fprintf('Time: %.2f s, Tms0: %.2f K, Tw1: %.2f K\n', t, Tms1_new, Tw1_new);
end

 % Create a 2x1 subplot for two plots
plot(time, Tms0_values);
xlabel('Time (s)');
ylabel('Temperature of Molten Salt (K)');
title('Temperature of Molten Salt vs. Time');
grid on;
% Plot the heat flux over time
 % Create the second plot in the 2x1 subplot
%plot(time, q_values);
%xlabel('Time (s)');
%ylabel('Heat flux (W/m2)')
%title('Heat flux vs. Time')
%grid on;
```

6.1.2. Heat Release

Listing 6.2: Check for release of heat

```
clear all
clc
% Heat loss without any insulation or pcm
% Constant values
m = 16145.50714; % mass of solar salt in the tank (kg)
cp_ms = 1596.46; % specific heat capacity of solar salt (J/kg.K)
cp_pcm = 1520; % specific heat capacity of pcm (J/kg.K)
Tms = 838; % intial temperature of the salt (K)
Rms =   0.00121482; % resistance of solar salt (W/m2K)
Rair = 0.103737411; % resistance of air (W/m2K)
Rpcm = 0.4464; % resistance of pcm (W/m2K)
area_ms = 18.85793876; % cross-section area of the tank (m2)
area_pcm = 18.85; % cross-section area of the pcm (m2)
Tair = 283; % ambient temperaute (K)
Tpcm = 626; % melting point of pcm
target_temp = 519.3; % melting point of solar salt (K)
delta_t = 60; %100; % time interval (seconds)
m_pcm = 1212; % 3090; % mass of pcm (kg)
syms Tms1_sym Tw1_sym Tpcm1_sym Tw2_sym;
time = [];
Tms0_values = [];
q_values = [];
% Initalize variables
Tms0 = Tms;
Tpcm0 = Tpcm;
t = 0;
while Tms0 > target_temp
  eq1 = -m*cp_ms*(Tms1_sym-Tms0)/delta_t == (Tms1_sym - Tw1_sym)/(Rms*(1/area_ms)); % heat loss equations
  eq2 = (Tms1_sym - Tw1_sym)/(Rms*(1/area_ms)) == (Tw1_sym - Tpcm1_sym)/(Rpcm*(1/area_pcm));
```

```
    eq3 = -m_pcm*cp_pcm*(Tpcm1_sym-Tpcm0)/delta_t == (Tw1_sym - Tw2_sym)/(Rpcm*(1/area_pcm)) - (Tms1_sym - Tw1_sym)/(Rms*(1/area_ms));
    eq4 = (Tw1_sym - Tw2_sym)/Rpcm == (Tw2_sym-Tair)/Rair;
    sol = vpasolve([eq1, eq2,eq3,eq4], [Tms1_sym, Tw1_sym, Tpcm1_sym, Tw2_sym]);
    Tms1_new = double(sol.Tms1_sym);
    Tw1_new = double(sol.Tw1_sym);
    Tpcm1_new = double(sol.Tpcm1_sym);
    Tw2_new = double(sol.Tw2_sym);

    % Update variables
    Tms0= Tms1_new;
    Tpcm0 = Tpcm1_new;
    t = t + delta_t;

    q =(Tms1_new - Tair) / (Rair + Rms);
    time = [time, t];  % Append the current time
    Tms0_values = [Tms0_values, Tms0];  % Append the current temperature
    q_values = [q_values, q];
    fprintf('Time: %.2f s, Tms0: %.2f K, Tw1: %.2f K, Tpcm0: %.2f K, Tw2: %.2f K\n', t, Tms1_new, Tw1_new, Tpcm1_new, Tw2_new);
end
```

6.1.3. Heat loss with PCM

```
 clear all
clc
% Heat loss without any insulation or pcm
% Constant values
m_ms = 16145.50714; % mass of solar salt in the tank (kg)
cp_ms = 1596.46; % specific heat capacity of solar salt (J/kg.K)
cp_pcm = 1520; % specific heat capacity of pcm (J/kg.K)
Tms = 838; % initial temperature of the salt (K)
Rms = 0.00121482; % resistance of solar salt (W/m2K)
Rair = 0.103737411; % resistance of air (W/m2K)
area = 18.85793876; % cross-section area of the tank (m2)
Tair = 283; % ambient temperature (K)
Tpcm = 626;%526;%576;%626; % melting point of pcm
target_temp = 519.3; % melting point of solar salt (K)
delta_t = 10; % time interval (seconds)
m_pcm = 10915;%4851; % 3090; % mass of pcm (kg)
hf = 230000; % latent heat of pcm (J/kg)
k_pcm = 0.56; % thermal conductivity of pcm (W/mK)
%Rpcm = 0.4464;
syms m_liq_pcm1_sym m_sol_pcm1_sym Tms1_sym Tw1_sym Tw2_sym;

time = [];
Tms0_values = [];
liq_frac = [];
q = [];

% Initialize variables
Tms0 = Tms;
m_sol_pcm0 = 0;
t = 0;
m_liq_pcm0 = m_pcm;
```

```
while Tms0 > target_temp

   if m_sol_pcm0 < m_pcm

        eq1 = -m_ms*cp_ms*(Tms1_sym-Tms0)/delta_t == (Tms1_sym - Tw1_sym)
           /(Rms*(1/area)); % heat loss equations
        eq2 = (Tms1_sym - Tw1_sym)/(Rms*(1/area)) == (Tw1_sym - Tpcm)
           /((0.25*(m_liq_pcm1_sym/m_pcm)/k_pcm)*(1/area));
        eq3 = ((m_sol_pcm1_sym - m_sol_pcm0)*hf)/delta_t == (Tpcm -
           Tw2_sym)/((0.25*(m_sol_pcm1_sym/m_pcm)/k_pcm)*(1/area)) - (
           Tw1_sym - Tpcm)/((0.25*(m_liq_pcm1_sym/m_pcm)/k_pcm)*(1/area));
        eq4 = (Tpcm - Tw2_sym)/(0.25*(m_sol_pcm1_sym/m_pcm)/k_pcm) == (
           Tw2_sym-Tair)/Rair;
        eq5 = m_pcm == m_liq_pcm1_sym + m_sol_pcm1_sym;

        sol = vpasolve([eq1, eq2, eq3, eq4, eq5], [m_liq_pcm1_sym,
           m_sol_pcm1_sym, Tms1_sym, Tw1_sym, Tw2_sym]);
    else
      eq1 = -m*cp_ms*(Tms1_sym-Tms0)/delta_t == (Tms1_sym - Tw1_sym)/(Rms
         *(1/area_ms)); % heat loss equations
      eq2 = (Tms1_sym - Tw1_sym)/(Rms*(1/area_ms)) == (Tw1_sym - Tpcm1_sym
         )/(Rpcm*(1/area_pcm));
      eq3 = -m_pcm*cp_pcm*(Tpcm1_sym-Tpcm0)/delta_t == (Tw1_sym - Tw2_sym)
         /(Rpcm*(1/area_pcm)) - (Tms1_sym - Tw1_sym)/(Rms*(1/area_ms));
      eq4 = (Tw1_sym - Tw2_sym)/Rpcm == (Tw2_sym-Tair)/Rair;
      sol2 = vpasolve([eq1, eq2,eq3,eq4], [Tms1_sym, Tw1_sym, Tpcm1_sym,
         Tw2_sym]);
      Tms1_new = double(sol.Tms1_sym);
      Tw1_new = double(sol.Tw1_sym);
      Tpcm1_new = double(sol.Tpcm1_sym);
      Tw2_new = double(sol.Tw2_sym);

   end
    % Extract solutions and ensure they are valid
    m_liq_pcm1_sol = double(sol.m_liq_pcm1_sym);
    m_sol_pcm1_sol = double(sol.m_sol_pcm1_sym);
    Tms1_sol = double(sol.Tms1_sym);
    Tw1_sol = double(sol.Tw1_sym);
    Tw2_sol = double(sol.Tw2_sym);

    % Check for real and valid physical values
    valid_indices = (imag(Tms1_sol) == 0) & (imag(Tw1_sol) == 0) & (imag(
       Tw2_sol) == 0) & (imag(m_liq_pcm1_sol) == 0) & (imag(m_sol_pcm1_sol
       ) == 0);
    valid_indices = valid_indices & (Tms1_sol > 0) & (Tw1_sol > 0) & (
       Tw2_sol > 0) & (m_liq_pcm1_sol > 0) & (m_sol_pcm1_sol > 0);

    % Select first valid solution
    if any(valid_indices)
        Tms1_new = Tms1_sol(valid_indices);
        Tms1_new = Tms1_new(1);

        Tw1_new = Tw1_sol(valid_indices);
        Tw1_new = Tw1_new(1);

        Tw2_new = Tw2_sol(valid_indices);
```

```
        Tw2_new = Tw2_new(1);

        m_liq_pcm1_sym_new = m_liq_pcm1_sol(valid_indices);
        m_liq_pcm1_sym_new = m_liq_pcm1_sym_new(1);

        m_sol_pcm1_sym_new = m_sol_pcm1_sol(valid_indices);
        m_sol_pcm1_sym_new = m_sol_pcm1_sym_new(1);
    else
        error('No valid solution found.')
    end

    % Update variables
    Tms0 = Tms1_new;
    m_sol_pcm0 = m_sol_pcm1_sym_new;
    t = t + delta_t;

     % Store results for plotting
    time(end + 1) = t;
    Tms0_values(end + 1) = Tms0;
    liq_frac(end + 1) =  m_liq_pcm1_sym_new/m_pcm ;


    fprintf('Time: %.2f s, Tms: %.2f K, Tw1: %.2f K, m_liq_pcm: %.2f kg,
       m_sol_pcm: %.2f kg, Tw2: %.2f K\n', t, Tms1_new, Tw1_new,
       m_liq_pcm1_sym_new, m_sol_pcm1_sym_new, Tw2_new);
end

   % Plot results


plot(time, liq_frac, 'LineWidth', 2);
xlabel('Time (s)');
ylabel('Liquid fraction (-)');
title('Liquid Fraction of PCM Over Time');
grid on;
```